PCCP

Catalytic Effect of Water and Formic Acid on the Reaction of Carbonyl Sulfide with Dimethyl Amine Under Tropospheric Conditions

Journal:	*Physical Chemistry Chemical Physics*
Manuscript ID	CP-ART-01-2021-000180.R2
Article Type:	Paper
Date Submitted by the Author:	11-Mar-2021
Complete List of Authors:	Arathala, Parandaman; University at Albany State University of New York, Chemistry Musah, Rabi; UAlbany-State University of New York, Chemistry

Catalytic Effect of Water and Formic Acid on the Reaction of Carbonyl Sulfide with Dimethyl Amine Under Tropospheric Conditions

Parandaman Arathala and Rabi A. Musah*

University at Albany—State University of New York, Department of Chemistry, 1400 Washington Avenue, Albany, NY 12222, USA

Abstract

CCSD(T)/aug-cc-pVTZ//M06-2X/aug-cc-pVTZ calculations were performed on the addition of amines [i.e. ammonia (NH_3), methyl amine (MA), and dimethyl amine (DMA)] to carbonyl sulfide (OCS), followed by transfer of the amine H-atom to either the S-atom or O-atom of OCS, assisted by a single water (H_2O) or a formic acid (FA) molecule, leading to the formation of the corresponding carbamothioic S- or O acids. For the OCS+NH_3 and OCS+MA reactions with or without the H_2O or FA, very high barriers were observed, making these reactions unfeasible. Interestingly, the barrier heights for the OCS+DMA reaction involving H-atom transfer to either the S-atom or O-atom of OCS and assisted by a FA, were found to be -4.2 kcal mol^{-1} and -3.9 kcal mol^{-1}, respectively relative to those of the separated reactants. The barrier height values suggest that FA lowers the reaction barriers by ~28.4 kcal mol^{-1} and ~35.9 kcal mol^{-1} compared to the OCS+DMA reaction without the catalyst. Rate coefficient calculations were performed on the OCS+DMA reaction both without a catalyst, and assisted by a H_2O and a FA molecule using canonical variational transition state theory and small curvature tunneling at the temperatures between 200 and 300 K. The rate data show that the OCS+DMA+FA reaction proceeds through H-atom transfer to the S-atom of OCS, which was found to be ~10^3-10^{11} and 10^3-10^{10} times faster than the OCS+DMA and OCS+DMA+H_2O reactions respectively in the studied temperature range. For the same temperature range, the rate of the OCS+DMA+FA reaction was found to be ~10^8-10^{16} and 10^3-10^{12} times faster than the OCS+DMA and OCS+DMA+H_2O reactions in which H-atom transfer to the O-atom of OCS occurred. This suggests that the OCS+DMA reaction that is assisted by FA is more efficient than the H_2O assisted reaction. In addition, the rate of the OCS+DMA+FA reaction was found to be ~10^{10} times slower than the OCS+•OH reaction at 298 K. This clarifies that the OCS+DMA+FA reaction may be feasible for the atmospheric removal of

OCS under night-time forest fire conditions when the OCS and DMA concentrations are high and the •OH concentration is low.

Keywords

carbonyl sulfide; dimethyl amine; catalyst; barrier height; rate coefficient; canonical variational transition state theory; small curvature tunneling.

*Corresponding Author.

E-mail address: rmusah@albany.edu

1. Introduction:

Carbonyl sulfide (OCS) is well-known as a long-lived sulfur containing atmospheric gas. It is considered to be a major S-carrier with an average mixing ratio of ~0.4 - 0.5 parts per billion (ppb) in the earth's troposphere,[1-6] and is believed to contribute sulfur mainly to the stratospheric aerosol layer.[7, 8] This has an adverse effect on stratospheric ozone and significantly impacts radiative balance of the atmosphere.[9] Various natural and anthropogenic sources are responsible for the OCS presence in the atmosphere.[10, 11] Primary emitters of OCS include soils, trees, marshes, plant roots, manure, microorganisms, biomass burning, volcanos, hot springs, and oceans.[12, 13] Importantly, oxidation of atmospheric dimethyl sulfide (Me_2S) and carbon disulfide (CS_2) generate up to one half of the terrestrial OCS as a secondary product in the global sulfur cycle.[13] Anthropogenic emissions which occur as a consequence of aluminum production, coal and automobile fuel burning, and industrial desulfurization, also contribute to global OCS production, albeit to a much lower extent.[14] Measurement of the OCS concentration in Antarctic ice cores suggests that its levels have risen over the past 350 years as a consequence of industrialization.[6]

The number of studies on removal processes of OCS from the atmosphere are limited. The major sink for this molecule is reported to be loss to vegetation through hydrolysis by the enzymes primarily involved in photosynthesis.[15-17] Another atmospheric loss process is its reaction with OH radicals. Various studies of the OCS + •OH reaction using experimental[18-21] and *ab initio* quantum chemistry methods[22-26] have been reported. Atkinson *et al.*[18] determined the rate coefficient for the OCS + •OH reaction using a flash photolysis resonance fluorescence technique and found an upper limit rate coefficient of 7.0×10^{-15} cm^3 $molecule^{-1}$ s^{-1} at 299 K. Using the same experimental technique, Kurylo determined the rate coefficient for the OCS + •OH reaction to be $(5.66 \pm 1.21) \times 10^{-14}$ cm^3 $molecule^{-1}$ s^{-1} at 296 K.[19] The study of this reaction by Cox and Sheppard[20] using

relative rate experiments furnished an upper limit rate coefficient of 4.0×10^{-14} cm^3 $molecule^{-1}$ s^{-1}. Ravishankara *et al.*[21] determined an upper limit rate coefficient at 298 K of 8.8×10^{-15} cm^3 $molecule^{-1}$ s^{-1} using a laser/flash photolysis resonance fluorescence technique. Using a similar experimental technique, Leu and Smith[27], Wahner and Ravishankara[28], and Cheng and Lee[29] determined room temperature rate coefficient values for the OCS + •OH reaction to be $(0.6 \pm 0.4) \times 10^{-15}$ cm^3 $molecule^{-1}$ s^{-1}; $(1.92 \pm 0.25) \times 10^{-15}$ cm^3 $molecule^{-1}$ s^{-1}; and $(2.0 \pm 0.8) \times 10^{-15}$ cm^3 $molecule^{-1}$ s^{-1}, respectively. Subsequently, using the relative rate technique combined with computational calculations, Schmidt *et al.*[30] reported the rate coefficient to be $(5.3 \pm 3.6) \times 10^{-15}$ cm^3 $molecule^{-1}$ s^{-1} at 296 K and 700 Torr.[30] The aforementioned rate coefficient results indicate that the OCS + •OH reaction is slow, and that its atmospheric lifetime with respect to •OH is from 2-4 years. Studies of additional atmospheric gas phase removal processes for OCS are required in order to learn more about the fate of this molecule in the atmosphere, since studies of alternative sinks for this molecule are very limited.

Amines are important atmospheric compounds due to their involvement in the formation of secondary organic aerosols (SOA) in the troposphere[31-34] and formation of amino acids in interstellar space.[35-37] The major sources of amines in the earth's atmosphere occur from both biogenic and anthropogenic emissions. These include motor vehicle exhaust, biomass burning, animal husbandry, industrial processes, and marine organisms.[31, 32] Atmospheric concentrations of amines such as methyl amine (CH_3NH_2, MA), and dimethyl amine ($(CH_3)_2NH$, DMA) are typically found in the range of parts per trillion by volume (pptv), to tens of pptv[38-40], while ammonia (NH_3) is typically at the tens of parts per billion by volume (ppbv) level.[41, 42] Several recent studies have shown that addition of amines to certain atmospherically important species results in formation of a new C-N bond, followed by H-atom transfer to yield various products,

and this has been shown to be an important removal pathway.[43-48] In this work, we investigated the possible atmospheric removal of OCS through its gas phase reaction with the three amines NH_3, MA, and DMA. In principle, these reactions can proceed by one of two possible pathways, given in eqns. 1 and 2.

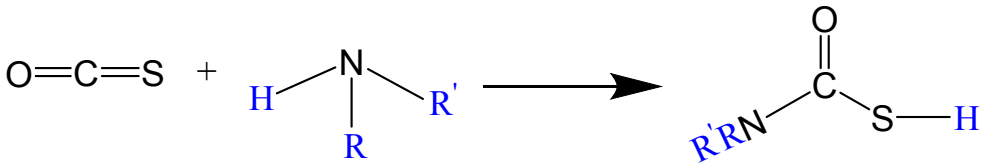

(1)

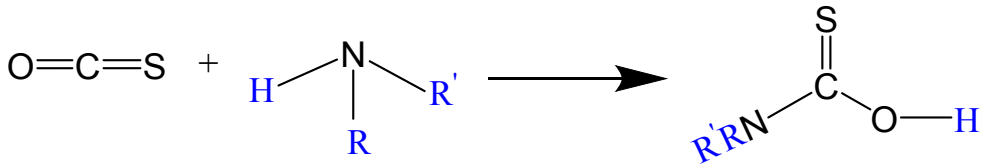

(2)

In eqns. 1 and 2, R and R' can be either −H or $-CH_3$, and both reactions proceed through nucleophilic addition of the N-atom to the C-atom of OCS. The subsequent step involves transfer of the amine H-atom to either the S-atom (eq. 1) or the O-atom (eq. 2) of OCS, leading to formation of the corresponding carbamothioic S- and O- acids respectively as final products.

It is well-known that water is the third most abundant species present in the atmosphere with a concentration of ~4.0 $\times 10^{17}$ molecules cm^{-3} at 298 K under 100% RH conditions. Yet another compound that has been found to be present in significant amounts is formic acid, which has been observed at the ~500 ppt level. Several studies have reported that water and formic acid form complexes with various atmospherically relevant volatile organic compounds (VOCs), volatile organosulfur compounds (VOSCs), and free radicals.[49-56] In addition, a number of studies have shown that single water and FA molecules successfully act as catalysts in reducing the energy barriers for several reactions, which in turn significantly influences reaction rates at atmospherically relevant temperatures and pressures.[55-57] Therefore, we also investigated the

single water (H_2O) and single formic acid (HC(O)OH, FA) molecule assisted catalysis of the reactions presented in eqns. 1 and 2 (i.e. eqns. 3 and 4), where X represents a catalyst (X = H_2O or FA).

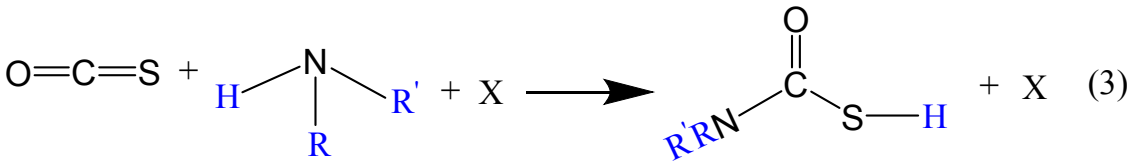

(3)

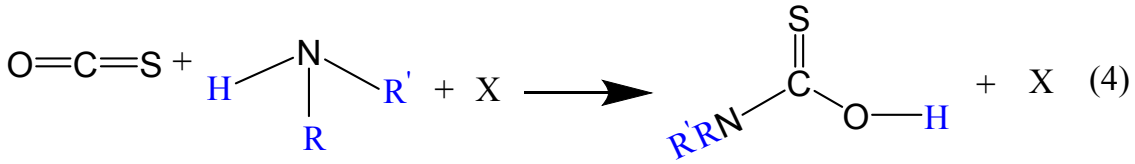

(4)

The energetics of the reactions presented in eqns. 1-4 were computed by quantum chemistry calculations. The results were then used to determine the rate coefficients with canonical variational transition state theory[58, 59] combined with small curvature tunneling.[60] This study also explored the effect of single water and single FA molecules on the reaction barrier heights, when compared to the reactions in the absence of a catalyst. The results from these investigations can provide insight into the reaction mechanism, energies, and reaction rates for amine addition reactions with OCS to form the corresponding carbamothioic acids in the troposphere.

2. Computational Methods:

High level *ab initio* quantum chemistry calculations were performed for the reaction of OCS with three amines in the absence and presence of a water and a FA as catalysts using the Gaussian-16 program suite.[61] Molecular geometry optimization of isolated reactants, pre-reactive complexes (PRCs), two body complexes (RCs), transition states (TSs), post-reactive complexes (PCs) and individual products involved in the present work was performed using the M06-2X

functional[62] in conjunction with the augmented correlation consistent polarized valence–triple-zeta basis set (aug-cc-pVTZ).[63, 64] The M06-2X method is a global hybrid meta generalized gradient approximation with 54% HF exchange, and it provides good results in calculations of thermochemistry and rate coefficients.[55, 65-68] Normal mode frequency calculations were performed at the same level of theory. All TSs were located using the OPT=TS routine of the Gaussian-16 program. The reactants, products, PRCs, RCs, and PCs all involved positive normal mode frequencies, and the TSs involved single imaginary frequencies. The optimized molecular geometries represent the minima on the respective potential energy surfaces (PESs). Intrinsic reaction coordinate (IRC) calculations[69] was performed at the M06-2X/aug-cc-pVTZ level for the TSs optimized at the same level of theory to confirm that the predicted TSs were connected with the corresponding PRCs and PCs. To improve the calculated energies for all the geometries optimized at the M06-2X/aug-cc-pVTZ level, we performed single point energy calculations at the CCSD(T) level with the same aug-cc-pVTZ basis set. Various studies have tested the combination of CCSD(T)/aug-cc-pVTZ//M06-2X/aug-cc-pVTZ (designated as CCSD(T)//M06-2X) level calculations for determining the energetics and rate coefficients for various atmospherically important reactions and it has been shown to be a reasonably accurate method.[70-72] The results obtained from T1 diagnostic calculations at the CCSD(T)/aug-cc-pVTZ level suggest that multi-reference character is not significant in the studied reactions.

The basis set superposition error (BSSE) might lead to increased stability of the pre-reactive complexes compared to the separated adducts. In this work, no BSSE corrections were performed because BSSE is difficult to treat in a uniform manner for all the complexes representing all the possible reaction paths. In addition, barrier heights for all the reaction paths were found to be ~5 – 45 kcal mol^{-1} above that of the pre-reactive complexes. This indicates that

the reaction barriers are large and hence the BSSE should be relatively small for the pre-reactive complexes studied here.

3. Results and Discussion:

3.1. Stationary points on the PESs and energetics:

3.1.1. The reaction of OCS with amines in the absence of a catalyst:

The present calculations were performed to determine the energies of OCS with three different amine addition reactions. The PES diagrams for the three selected amines, (NHRR', where R and R' refer to either -H or -CH_3), namely NH_3, MA, and DMA involved in each addition pathway with OCS leading to the formation of the corresponding carbamothioic acid (see eqns. 1 and 2) are shown in Figure 1a-b. All the stationary point energies on the PESs were calculated at the CCSD(T)//M06-2X level. In Figure 1a, the symbols RC1, TS1, and P_1 correspond to the OCS + NH_3 reaction; RC2, TS2, and P_2 correspond to the OCS + MA reaction; and RC3, TS3, and P_3 correspond to the OCS + DMA reaction, respectively.

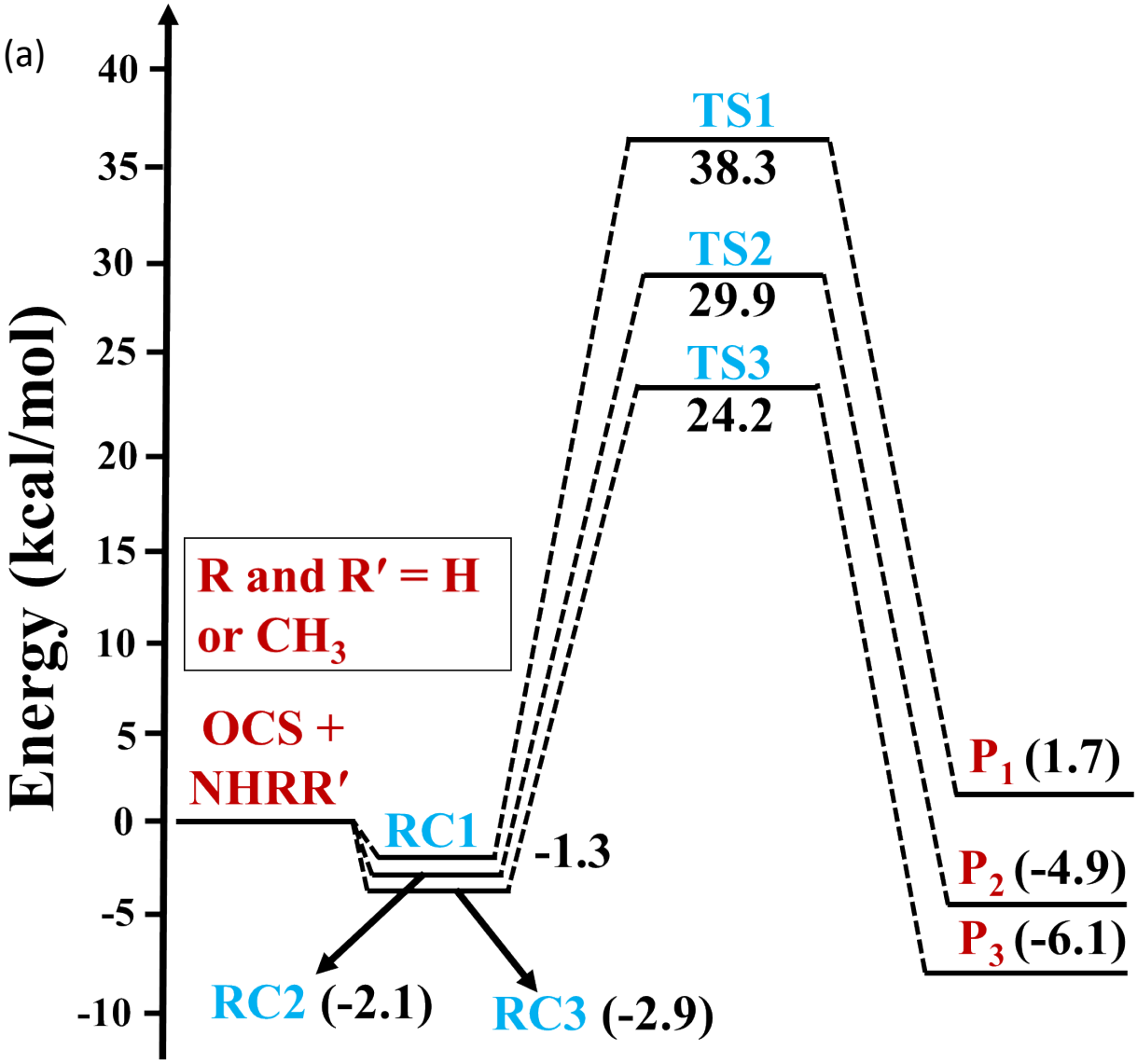
(a)
Energy (kcal/mol)
40
35
30
25
20
15
10
5
0
-5
-10
TS1
38.3
TS2
29.9
TS3
24.2
R and R′ = H
or CH3
OCS +
NHRR′
RC1
-1.3
RC2 (-2.1)
RC3 (-2.9)
P1 (1.7)
P2 (-4.9)
P3 (-6.1)

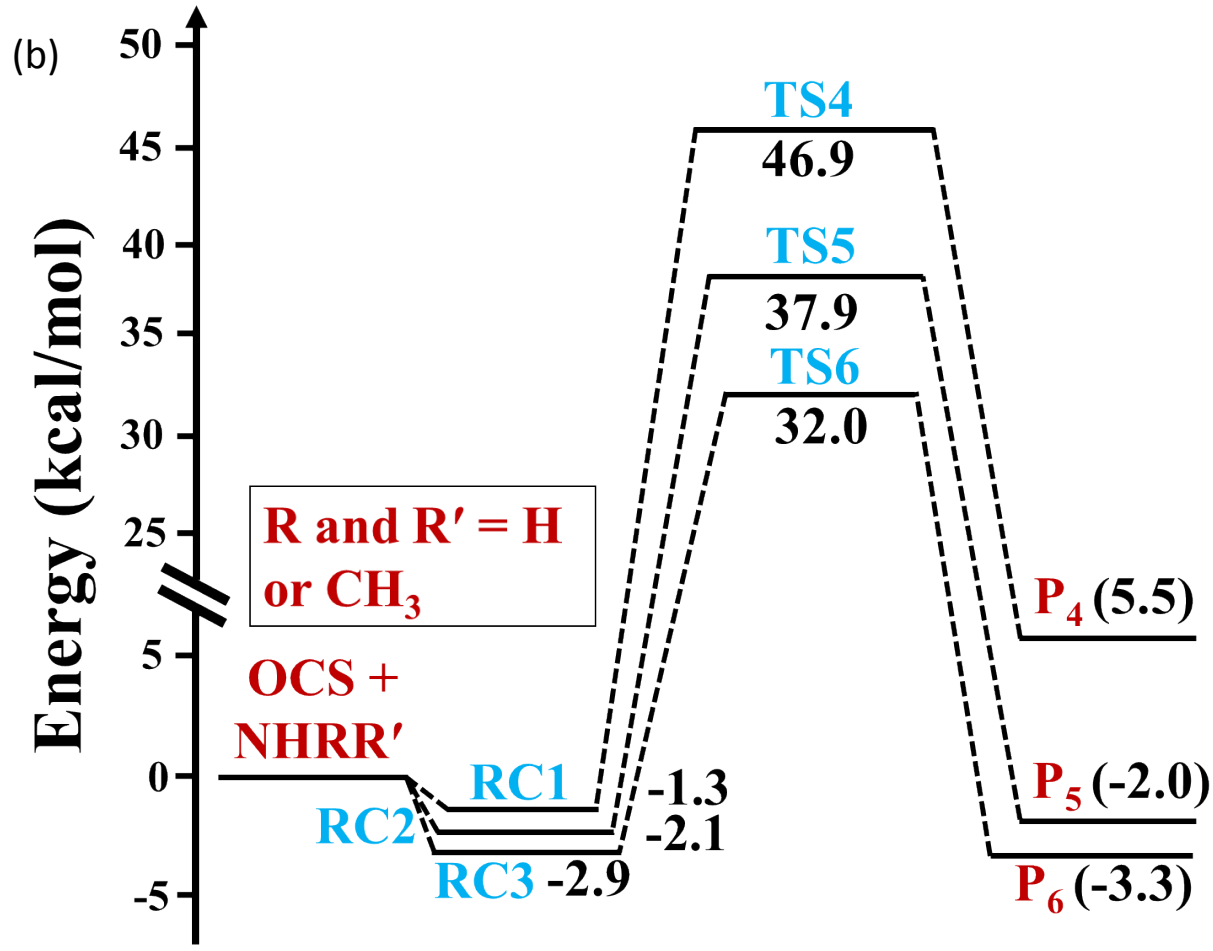

Figure 1. Potential energy surface diagrams for: (a) addition of three different amines to OCS followed by transfer of the amine hydrogen atom to the S-atom of OCS; and (b) addition of three different amines to OCS followed by transfer of the amine hydrogen atom to the O-atom of OCS. The energies of all minima on the PESs were obtained at the CCSD(T)/aug-cc-pVTZ//M0-62X/aug-cc-pVTZ level. The symbols RC_n (n = 1-3), TS_n (n = 1-6), and P_n (n = 1-6) refer to dimer complexes, transition states, and carbamothioic acid products, respectively.

The computed total electronic energies (E_{total}) and zero-point energy (ZPE) corrected electronic energies [E_{total}(ZPE)] for all the minima obtained at the M06-2X and CCSD(T) levels are given in Table S1. The geometries, imaginary frequencies of the various TSs, vibrational frequencies and rotational constants obtained in this work are provided in Tables S2-S5. The

optimized geometries of the reactants, RCs, PRCs, TSs, PCs, and products involved in the OCS + NH_3 and OCS + MA reactions both without a catalyst and assisted by H_2O and FA single molecules are shown in Figure S1 and S2 of the supporting information. The PES profile shown in Figure 1a suggests that each amine addition with OCS proceeds via the formation of a two-body complex (RC1, RC2, and RC3) that is below the separated reactants. The formed RCs proceed to the corresponding three transition states (TS1, TS2, and TS3) via addition of the amine N-atom to the C-atom of OCS, forming a new C-N bond, followed by simultaneous transfer of hydrogen from the amine hydrogen to the S-atom of OCS (see Figure S1). The barrier heights for the formation of TS1, TS2, and TS3 were computed to be 38.3, 29.9, and 24.2 kcal mol^{-1}, respectively, above that of the starting reactants. The formed TSs proceed further to form carbamothioic acid (P_1), *N*-methyl carbamothioic acid (P_2), and *N,N*-dimethyl carbamothioic acid (P_3), as products from the reaction of ammonia, MA and DMA respectively. The barrier heights presented in Figure 1a indicate that the reaction of OCS with DMA to form P_3 is the most energetically feasible, as it was found to differ from those of the OCS + NH_3 and OCS + MA reactions by ~14.1 and ~5.7 kcal mol^{-1} respectively.

Next, calculations were performed for the reaction of each of the three amines to OCS, in which nucleophilic addition of nitrogen to carbon is followed by H-atom transfer to the O-atom of OCS to form the corresponding products. The PES diagram obtained at the CCSD(T)//M06-2X level is shown is Figure 1b. The symbols RC1, TS4, and P_4 correspond to the OCS + NH_3 reaction; RC2, TS5, and P_5 correspond to the OCS + MA reaction; and RC3, TS6, and P_6 correspond to the OCS + DMA reaction, respectively. From this Figure, each addition reaction pathway proceeds via formation of RC1, RC2, and RC3, which then form the corresponding transition states (TS4, TS5, and TS6) with barrier heights of 46.9, 37.9, and 32.0 kcal mol^{-1}, respectively. The formed

TSs lead to the formation of the corresponding products (P_4, P_5, and P_6), respectively. The barrier heights shown in Figure 1b indicate that the DMA + OCS reaction via TS6 is lower than those of the OCS + NH_3 (TS4) and OCS + MA (TS5) reactions by ~15.0 and ~6.0 kcal mol^{-1} respectively. Overall, the calculated barrier heights for the OCS + amine addition reactions are found to be very high (see Figure 1a-b) and require high energies. While the reaction that proceeds by eq. 1 is more energetically favorable, neither of the reactions in eqs. 1 or 2 is feasible under normal tropospheric temperatures and pressures.

3.1.2. The reaction of OCS with NH_3 assisted by a single H_2O molecule:

Water (H_2O) and formic acid (FA) are two important and ubiquitous molecules that are present in significant amounts in the troposphere.[43, 55, 56] Both have been previously shown to catalyze various atmospherically important reactions.[43, 44, 48, 55, 56] Therefore, we investigated the energetics of the three amine addition reactions at the CCSD(T)//M06-2X level to determine the potential impact of single H_2O and FA molecules on the atmospheric removal of OCS. First, the OCS + NH_3 reaction assisted by a single H_2O molecule and leading to the formation of the corresponding carbamothioic acid was investigated. The obtained PES profiles involving all the minima for the two possible reaction channels (i.e. eqs. 3 and 4) are shown in Figure 2, which illustrates the addition of ammonia to the C-atom of OCS, followed by H-atom transfer to the S- or O-atom of OCS, assisted by a single H_2O molecule. The energies indicated on the PES profiles were calculated at the CCSD(T)//M06-2X level.

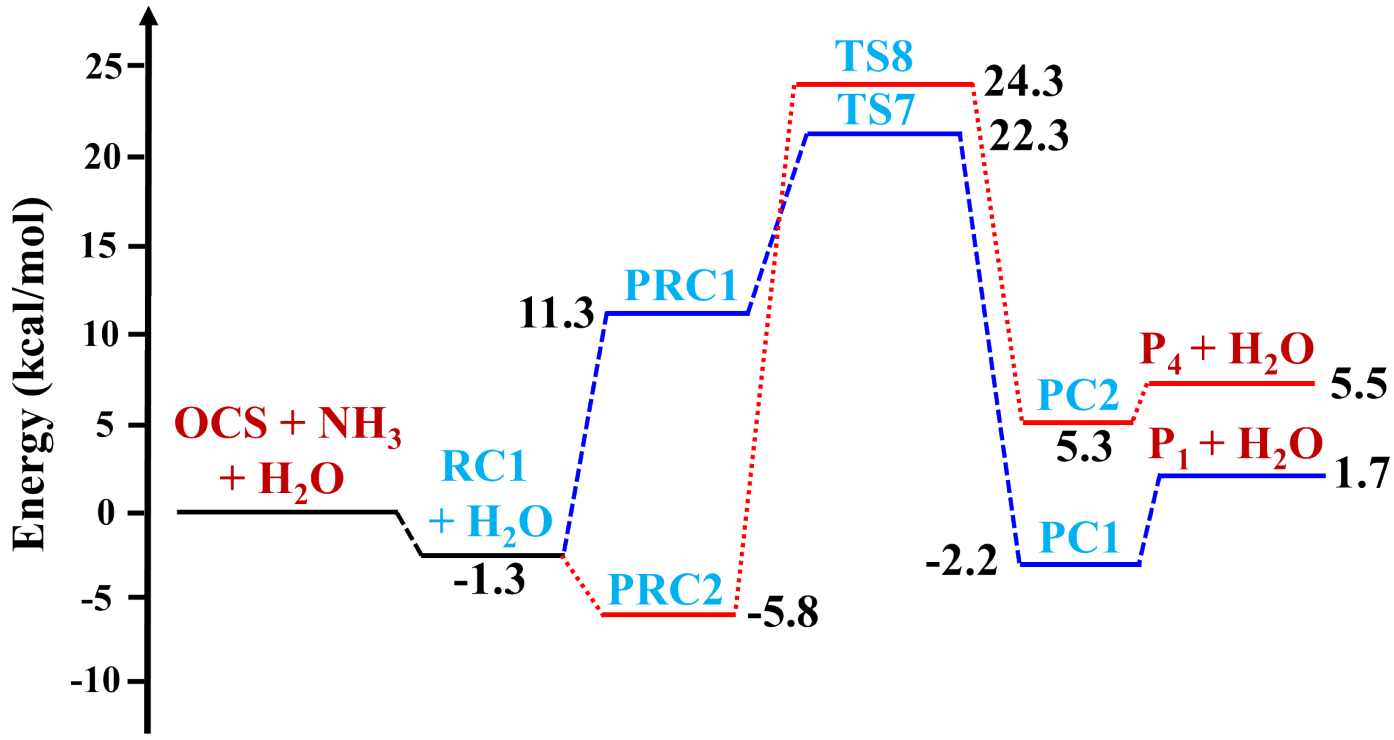

Figure 2. The CCSD(T)/aug-cc-pVTZ//M0-62X/aug-cc-pVTZ calculated potential energy surface diagram for the addition of ammonia to OCS followed by migration of the H-atom to either the S-atom (indicated using blue lines) or O-atom (indicated using red lines) of the OCS catalyzed by a single H_2O molecule to form carbamothioic acid. The symbols RC1; PRC1 and PRC2; TS7 and TS8; PC1 and PC2; and P_1 and P_4 refer to the OCS••NH_3 dimer complex, the pre-reactant complexes, the transition states, the post-reactive complexes, and the carbamothioic acid products, respectively.

Figure 2 shows that the OCS + NH_3 reaction catalyzed by a H_2O molecule initially leads to the formation of a OCS••NH_3 complex (RC1) with a binding energy of ~1.3 kcal mol^{-1} below that of the starting reactants. The complex then reacts with a H_2O molecule leading to the formation of a pre-reactant complex (PRC1) at 11.3 kcal mol^{-1} above the starting reactants. The reaction further proceeds from PRC1 to the formation of a transition state (TS7) with a barrier height of 22.3 kcal mol^{-1} relative to that of the starting reagents. The structure of TS7 shows addition of the N-atom

of ammonia to the C-atom of OCS, followed by transfer of the ammonia H-atom to the O-atom of H_2O and then to the S-atom of OCS (see Figure S1). TS7 continues through formation of the post reactive complex (PC1) and then to the formation of carbamothioic acid (P1) + H_2O as final products. The barrier height for this reaction reveals that in comparison to the reaction in the absence of water, the presence of a single H_2O molecule reduces the transition state energy by ~16.0 kcal mol^{-1}.

The reaction of ammonia addition to the C-atom of OCS followed by H-atom migration to the O-atom of OCS, assisted by a single H_2O molecule is also shown in Figure 2. This pathway also occurs via OCS••NH_3 (RC1) + H_2O leading to the formation of a pre-reactant complex (PRC2) with an energy of ~5.8 kcal mol^{-1} below that of the starting reactants. The formed PRC2 proceeds to a transition state (TS8) with a barrier height of 24.3 kcal mol^{-1} with respect to the starting OCS + NH_3 + H_2O reactants. The formation of TS leads to the corresponding post-reactive complex (PC2) and then on to form carbamothioic acid (P_4) + H_2O as final products (see Figure 2). Therefore, the presence of a H_2O molecule lowers the barrier height for the OCS + NH_3 reaction by ~22.6 kcal mol^{-1} when compared to the value of the same reaction in the absence of the catalyst.

3.1.3. The reaction of OCS with NH_3 assisted by a single HC(O)OH molecule:

We next examined the impact on the barrier height of the OCS + NH_3 reaction of a single FA molecule in place of a H_2O molecule. The obtained PES profiles involving all the minima are shown in Figure 3. Like the OCS + NH_3 + H_2O reaction, OCS + NH_3 + FA also progresses through the OCS••NH_3 + FA reaction, leading to formation of a pre-reactant complex (PRC3). The reaction then proceeds further to form a transition state (TS9) with a barrier height of ~9.8 kcal mol^{-1} above that of the starting reactants. The TS structure for this reaction suggests that it proceeds via addition of the ammonia N-atom to the C-atom of OCS, followed by transfer of the ammonia H-atom to

the O-atom of FA and then to the S-atom of OCS. The reaction continues by forming a post reactive complex (PC3), which then undergoes unimolecular decomposition to form final products (P_1 + FA). Similarly, the addition of ammonia to OCS followed by an H-atom shift towards the O-atom of OCS assisted by a FA molecule, also proceeds from the OCS••NH_3 + FA reaction to form the corresponding pre-reactant complex (PRC4), and then to transition state (TS10) with a corresponding barrier height of ~9.0 kcal mol^{-1}. The reaction then proceeds further via PC4 and then to final products (P_4 + FA). The results for the reaction of OCS + NH_3 assisted by FA suggest that a FA molecule reduces the barrier height for the H-atom transfer to the S-atom of OCS by ~28.5 kcal mol^{-1} and ~12.5 kcal mol^{-1} compared to the uncatalyzed and single H_2O catalyzed reactions. For the alternative reaction path (H-atom transfer to the O-atom of OCS), a single FA molecule reduces the barriers by ~37.9 kcal mol^{-1} and ~15.3 kcal mol^{-1} compared to the uncatalyzed and water catalyzed reactions.

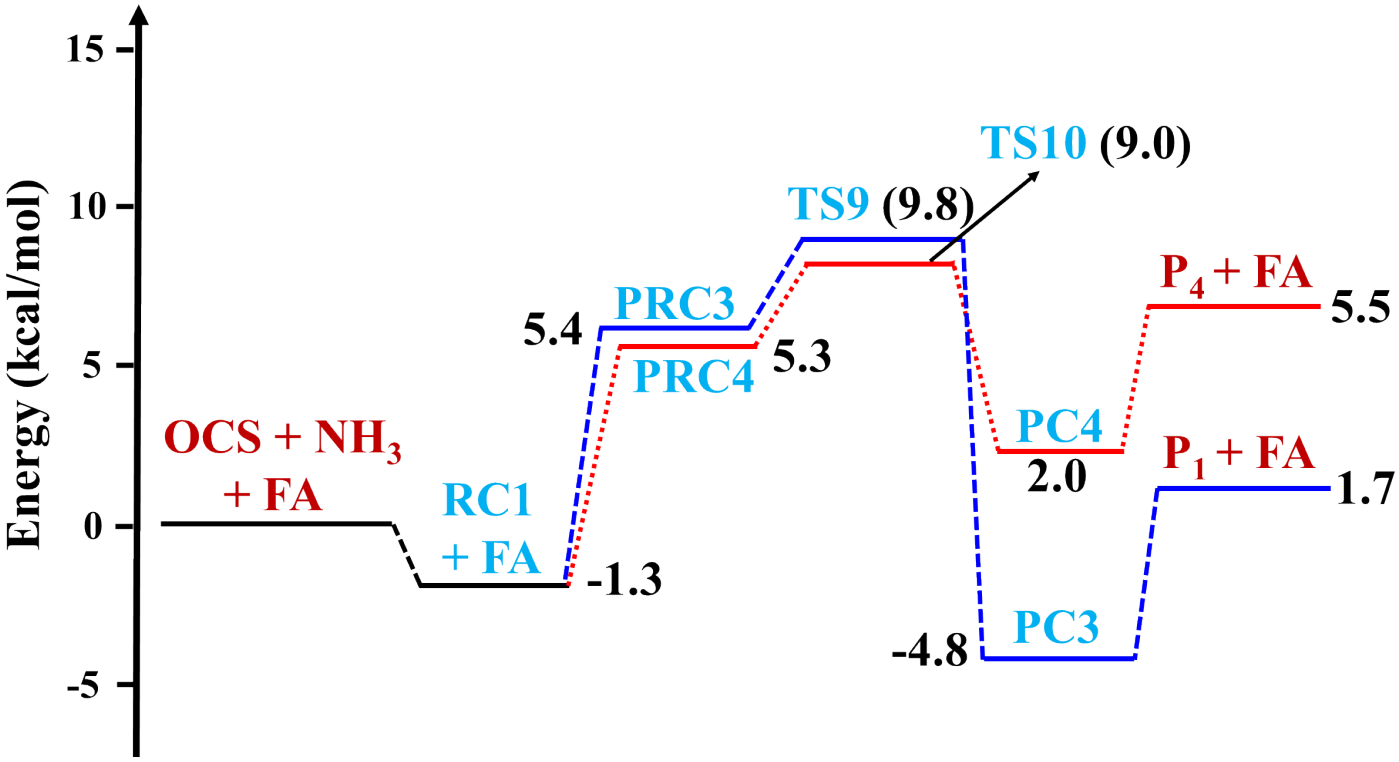

Figure 3. The CCSD(T)/aug-cc-pVTZ//M0-62X/aug-cc-pVTZ calculated potential energy surface diagram for the addition of ammonia to OCS followed by migration of the H-atom to either the S-atom (indicated with blue lines) or O-atom (indicated with red lines) of OCS catalyzed by a formic acid to form carbamothioic acid. The symbols RC1; PRC3 and PRC4; TS9 and TS10; PC3 and PC4; and P_1 and P_4 refer to the OCS••NH_3 dimer complex, the pre-reactant complexes, the transition states, the post-reactive complexes, and the carbamothioic acid products, respectively.

3.1.4. The reaction of OCS with $(CH_3)NH_2$ assisted by a single H_2O molecule:

We also performed calculations on the addition of MA to OCS that is followed by H-atom transfer from the -NH_2 moiety to either the S- or O-atoms of OCS, assisted by a single H_2O molecule. The PESs involving all the minima for the two possible reaction paths obtained at the CCSD(T)//M06-2X level are shown in Figure 4, which illustrates the energies for of the minima on the PESs that were estimated relative to the OCS + MA + H_2O starting reagents.

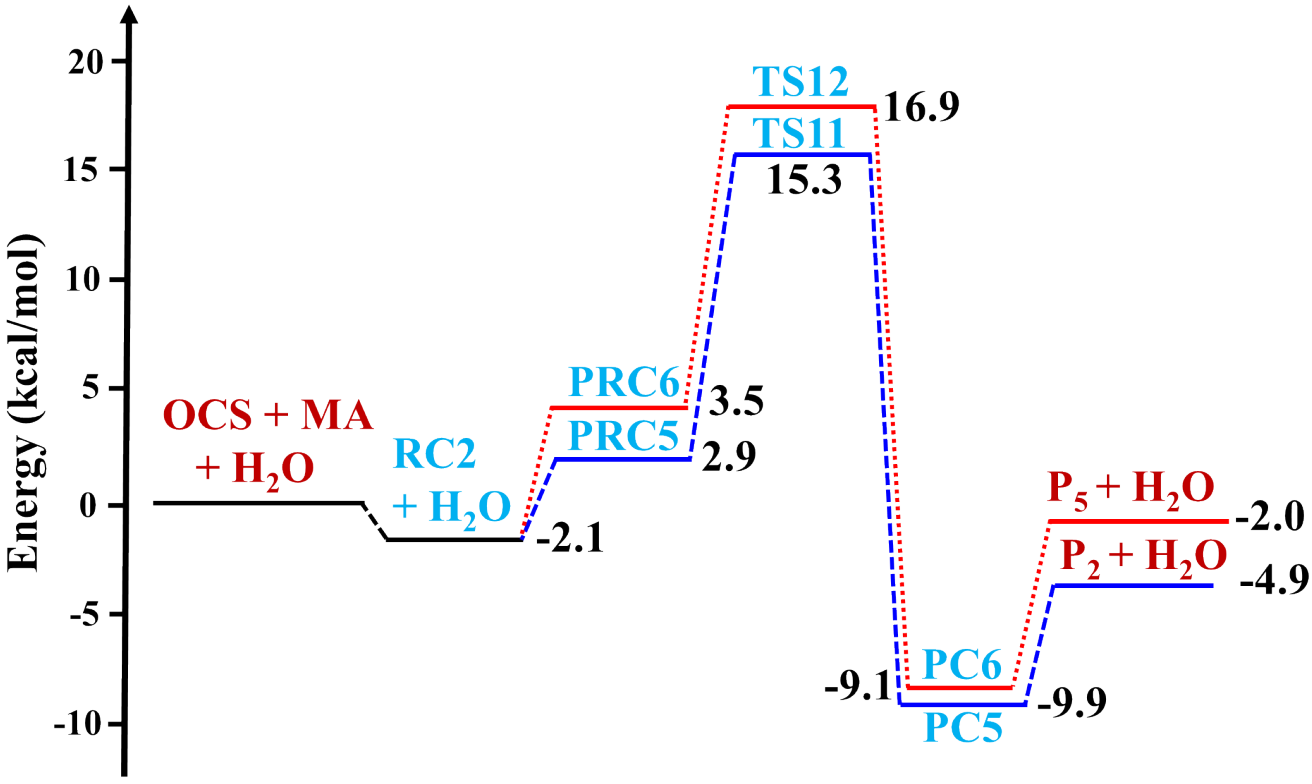

Figure 4. The CCSD(T)/aug-cc-pVTZ//M0-62X/aug-cc-pVTZ calculated potential energy surface diagram for the addition of methyl amine to OCS followed by migration of the H-atom to either the S-atom (indicating using blue lines) or O-atom (indicated using red lines) of OCS catalyzed by a single H_2O molecule to form *N*-methyl carbamothioic acid. The symbols RC2; PRC5 and PRC6; TS11 and TS12; PC5 and PC6; and P_2 and P_5 refer to the OCS••MA complex, the pre-reactant complexes, the transition states, the post reactive complexes, and the *N*-methyl carbamothioic acid products, respectively.

The OCS + MA + H_2O reaction initially proceeds through the bimolecular interaction of OCS••MA (RC2) with a H_2O molecule, leading to the formation of a pre-reactant complex (PRC5). The reaction then progresses to the formation of a transition state (TS11) from PRC5 with a barrier height of ~15.3 kcal mol^{-1} relative to that of the starting reactants. TS11 advances to formation of PC5 and then on to form *N*-methyl carbamothioic acid (P_2) + H_2O as products. Similarly, the alternative pathway proceeds from OCS••MA (RC2) + H_2O to form PRC6, which then proceeds to form TS12 with a barrier height of ~16.9 kcal mol^{-1} above that of the starting reactants. A post reactive complex (PC6) forms from TS12 which then leads to the formation of P_5 + H_2O as products. Therefore, for the MA + OCS reaction that proceeds via addition of the amine N-atom followed by H-atom transfer from nitrogen to either the S- or O-atom of OCS, a single H_2O molecule reduces the barrier heights by ~14.6 kcal mol^{-1} and ~21 kcal mol^{-1} respectively when compared to the same reaction in the absence of water.

3.1.5. The reaction of OCS with $(CH_3)NH_2$ assisted by a single HC(O)OH molecule:

Similarly, calculations on the OCS + MA reaction assisted by a single FA molecule were performed at the CCSD(T)//M06-2X level, and the observed PES is shown in Figure 5. The reaction begins with the OCS + MA + FA reactants by forming a OCS••MA (RC2) dimer, which

then reacts with FA, leading to the formation of two different pre-reactive complexes (PRC7 and PRC8) with binding energies of ~3.3 and ~4.1 kcal mol^{-1} below that of the starting reactants. PRC7 and PRC8 further proceed to form the corresponding transition states (TS13 and TS14) with barrier heights of 1.0 kcal mol^{-1} and -0.2 kcal mol^{-1} respectively when compared to that of the starting reactants. These two pathways further proceed to form the corresponding post-reactive complexes (PC7 and PC8) and then on to form the corresponding bimolecular products P_2 + FA and P_5 + FA respectively. Therefore, the present calculations suggest that a single FA reduces the TS barrier heights for the H-atom transfer to the S-atom of OCS by ~29 kcal mol^{-1} and ~14.3 kcal mol^{-1}, whereas for H-atom transfer to the O-atom of OCS, the barrier heights are reduced by ~38.1 kcal mol^{-1} and 17.1 kcal mol^{-1} compared to the values for OCS + MA in the absence and presence of a single water molecule respectively.

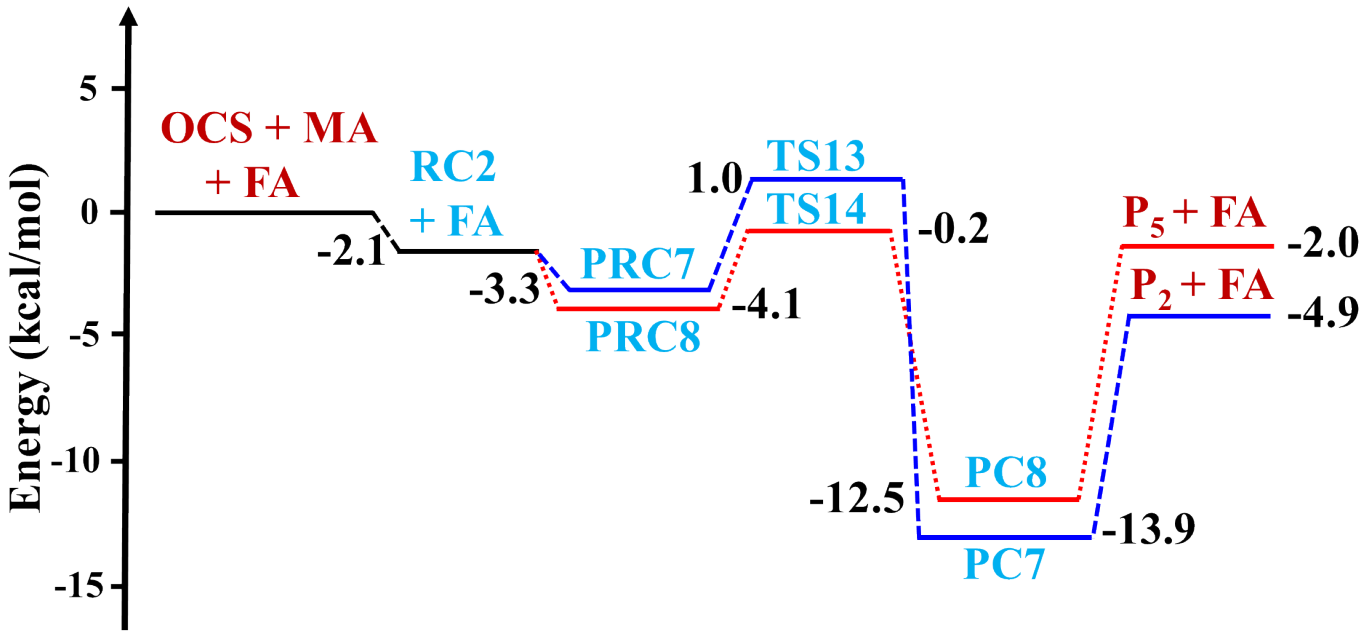

Figure 5. The CCSD(T)/aug-cc-pVTZ//M0-62X/aug-cc-pVTZ calculated potential energy surface diagram for the addition of methyl amine to OCS followed by migration of the H-atom to either the S-atom (indicated with blue lines) or O-atom (indicated with red lines) of OCS catalyzed by a

formic acid to form *N*-methyl carbamothioic acid. The symbols RC2; PRC7 and PRC8; TS13 and TS14; PC7 and PC8; and P_2 and P_5 refer to the OCS••MA dimer complex, the pre-reactant complexes, the transition states, the post reactive complexes, and the *N*-methyl carbamothioic acid products, respectively.

3.1.6. The reaction of OCS with $(CH_3)_2NH$ assisted by a single H_2O molecule:

We next examined the OCS + DMA reaction catalyzed by a single water molecule. The simultaneous collision of three reactant species (OCS, DMA, and H_2O) in the atmosphere is not feasible. Therefore, the OCS + DMA + H_2O reaction was considered as taking place through the collision of a dimer complex with another reactant species. Accordingly, the OCS + DMA + H_2O reaction was modelled to occur via the three bimolecular reaction paths given in eqns. 5-7.

$$OCS\bullet\bullet DMA + H_2O \rightarrow HS\text{-}C(=O)N(CH_3)_2 + H_2O \quad (5)$$

$$OCS\bullet\bullet H_2O + DMA \rightarrow HS\text{-}C(=O)N(CH_3)_2 + H_2O \quad (6)$$

$$DMA\bullet\bullet H_2O + OCS \rightarrow HS\text{-}C(=O)N(CH_3)_2 + H_2O \quad (7)$$

The CCSD(T)//M06-2X calculated PES profiles for the OCS + DMA + H_2O reaction are shown in Figure 6 and the optimized geometries of all the stationary points at the M06-2X/aug-cc-pVTZ level are shown in Figure 7. The DMA••H_2O + OCS reaction (eqn. 7) was not considered further because the structure of the DMA••H_2O complex (RC6) (see Figure 7) clearly shows the existence of a hydrogen bond between the N-atom of DMA and the H-atom of H_2O, which blocks the N-atom from attacking the C-atom of OCS. Therefore the OCS + DMA + H_2O reaction could in principle proceed via eqns. 5 and 6. The PES for the OCS + DMA + H_2O reaction shows that the reaction initially forms three different dimer complexes: OCS••DMA (RC3); OCS••H_2O (RC4); and OCS••H_2O (RC5) with binding energies below that of the starting reactants of ~2.9, ~1.0, and

~1.2 kcal mol^{-1} respectively. The formed OCS••DMA (RC3) and OCS••H_2O (RC4) dimer complexes further react with H_2O and DMA reactants. The reaction then leads to formation a pre-reactant complex (PRC9) with an energy of ~2.4 kcal mol^{-1} below that of the initial starting reactants. PRC9 proceeds through the addition of DMA to OCS followed by transfer of the H-atom of the -NH moiety to the S-atom of OCS with help of a H_2O molecule to form a transition state (TS15) with a barrier height of ~11.3 kcal mol^{-1}. The reaction further advances through the formation of a post-reactive complex (PC9) and then on to the formation of *N,N*-dimethyl carbamothioic acid (P_3) + H_2O products.

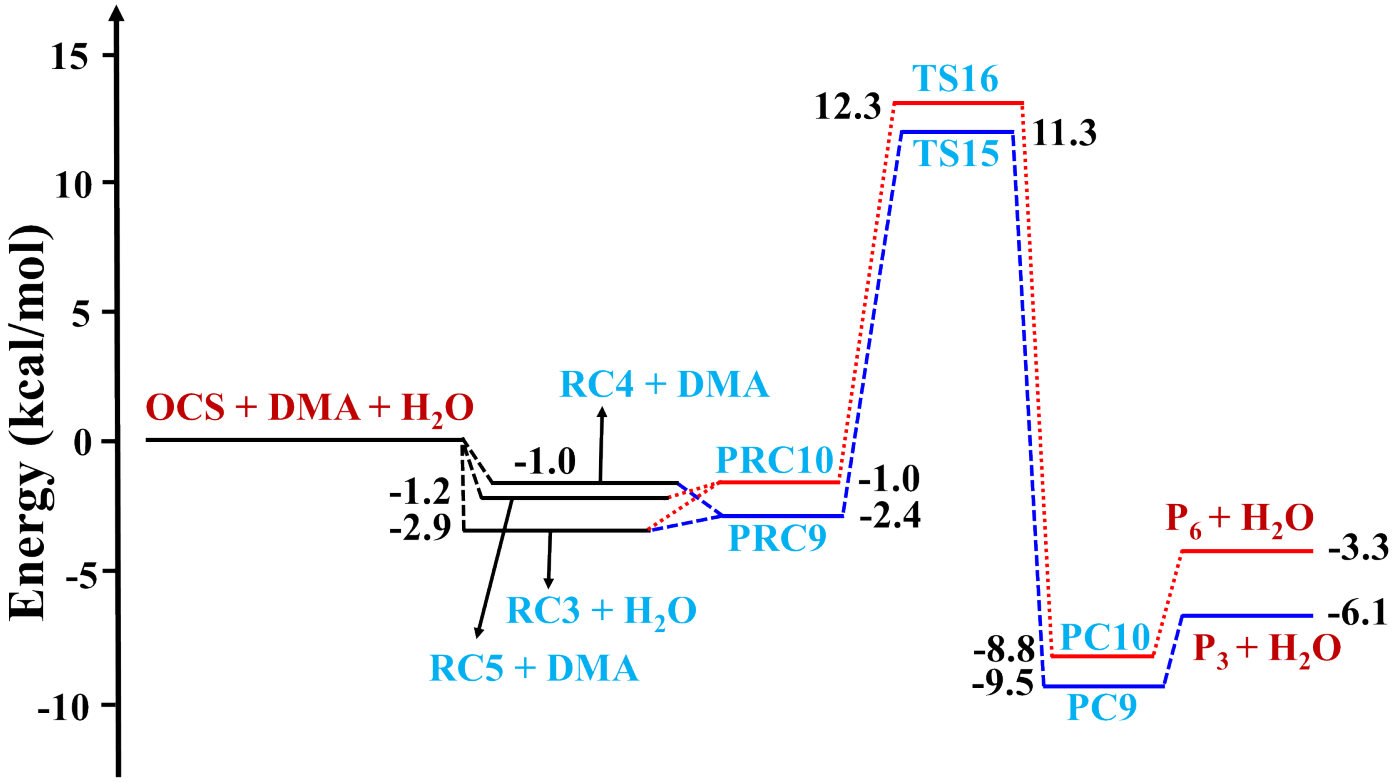

Figure 6. The CCSD(T)/aug-cc-pVTZ//M0-62X/aug-cc-pVTZ calculated potential energy surface diagram for the addition of dimethyl amine to OCS followed by migration of the H-atom to either the S-atom (indicated using blue lines) or O-atom (indicated using red lines) of OCS catalyzed by a single water molecule to form *N,N*-dimethyl carbamothioic acid. The symbols RC3, RC4 and RC5; PRC9 and PRC10; TS15 and TS16; PC9 and PC10; and P_3 and P_6 refer to the dimer

complexes, the pre-reactant complexes, the transition states, the post reactive complexes, and the *N,N*-dimethyl carbamothioic acid products, respectively.

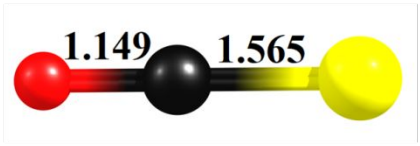

OCS

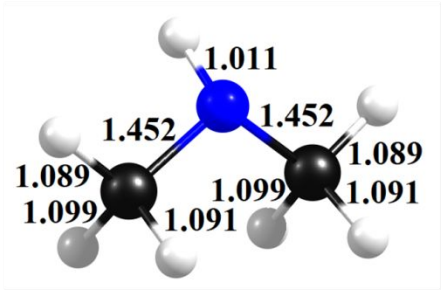

DMA

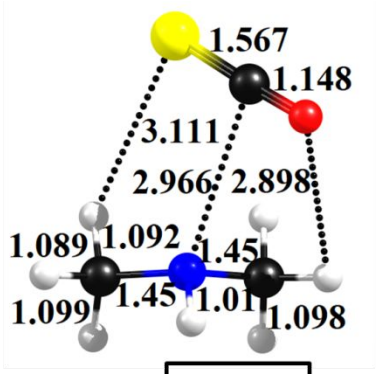

RC3

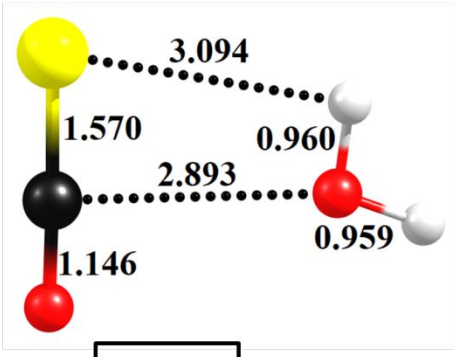

RC4

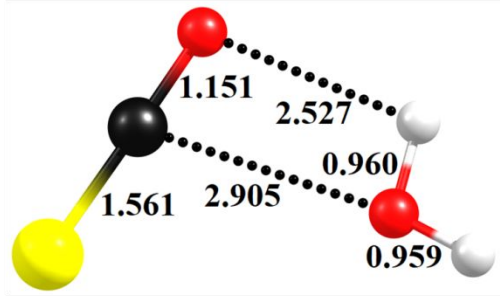

RC5

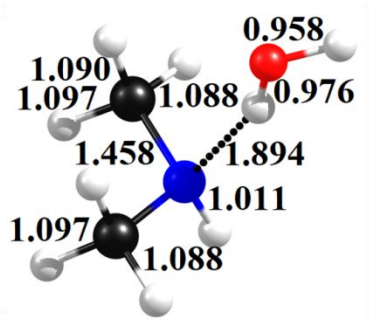

RC6

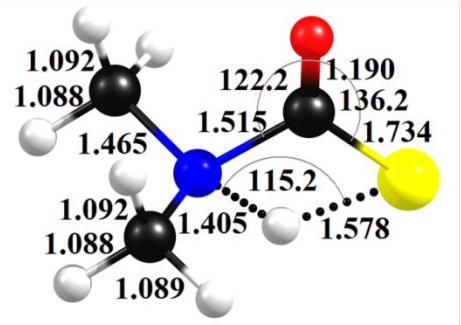

TS3

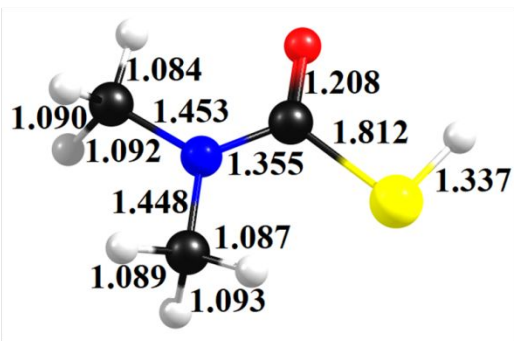

P_3

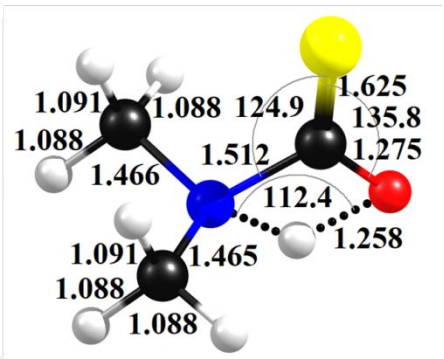

TS6

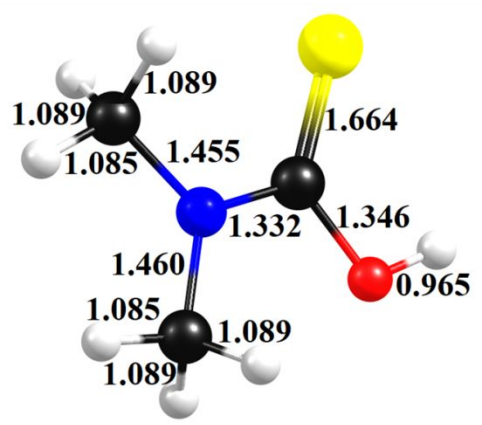

P_6

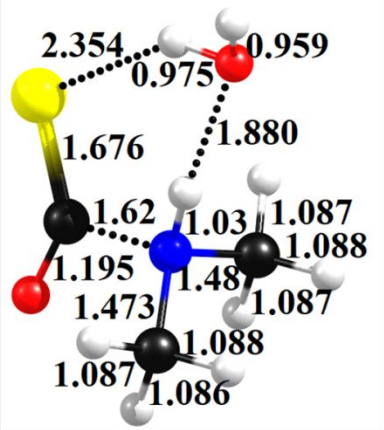

PRC9

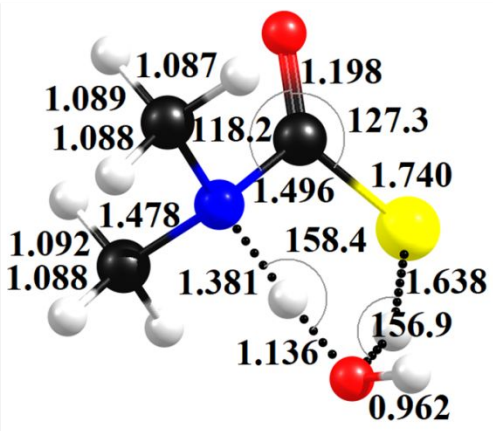

TS15

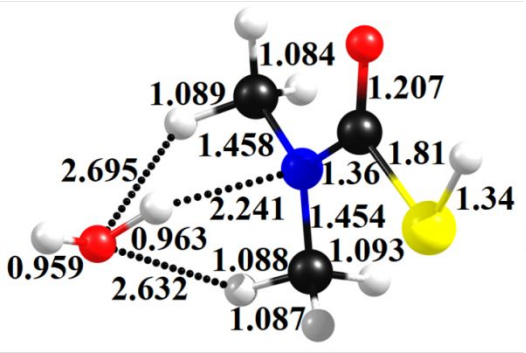

PC9

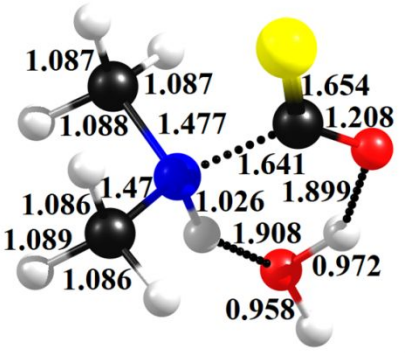

PRC10

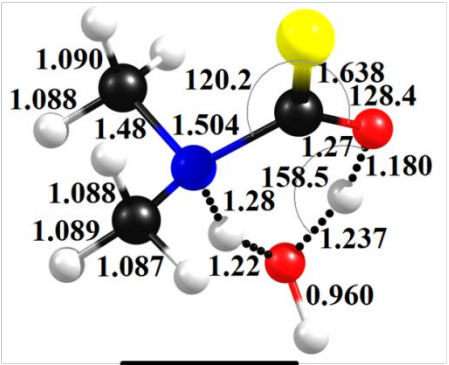

TS16

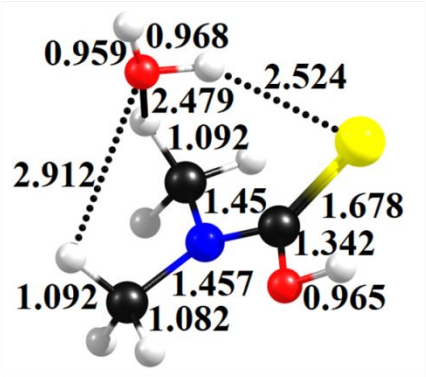

PC10

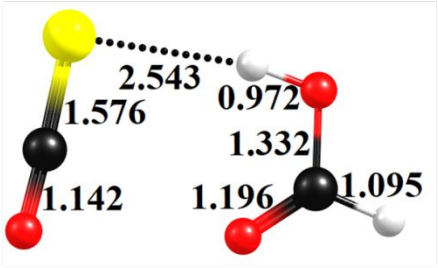

RC7

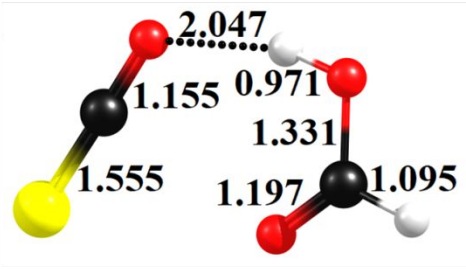

RC8

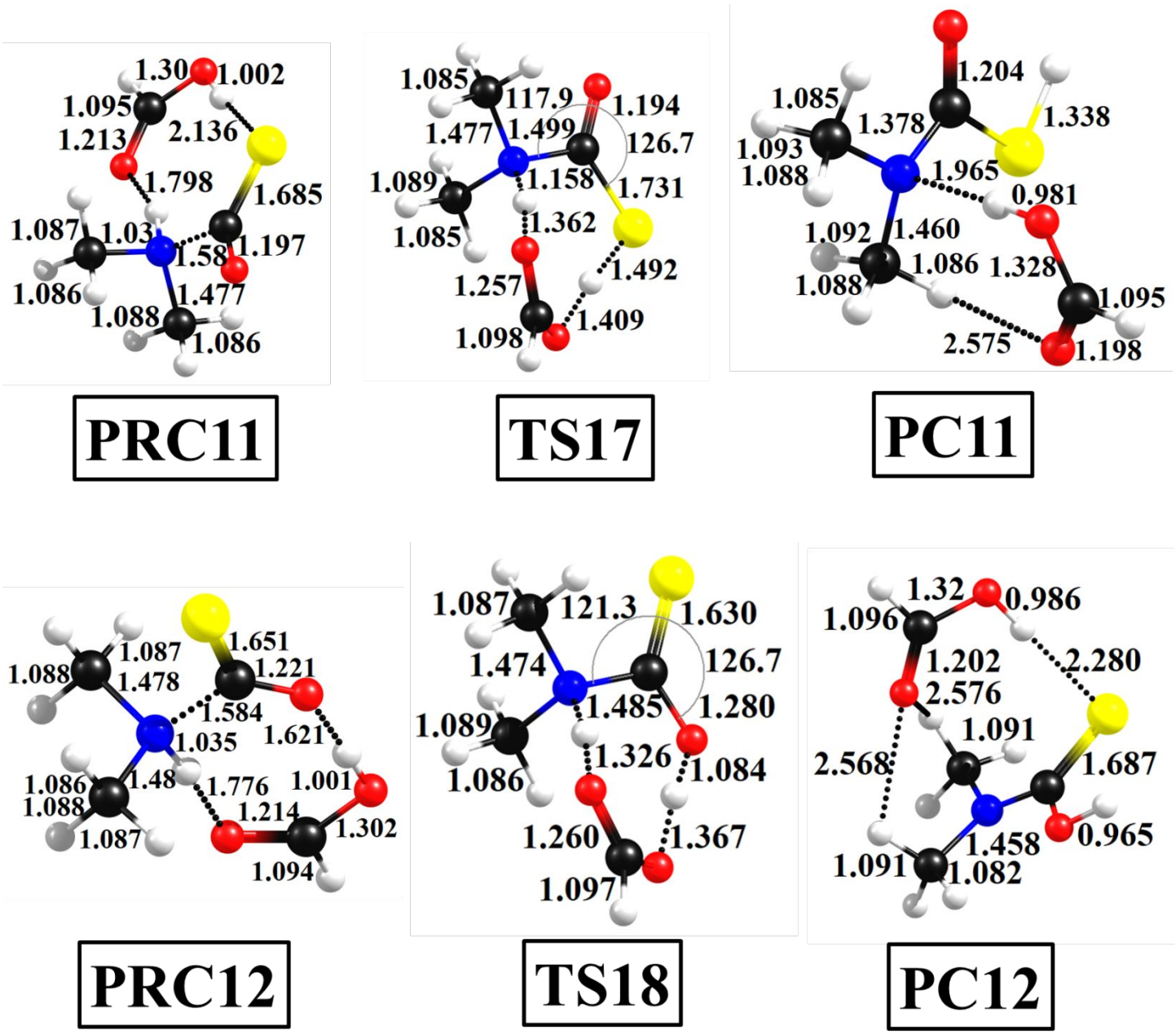

Figure 7. The M06-2X/aug-cc-pVTZ optimized geometries for the addition of dimethyl amine to OCS without a catalyst and assisted by a water and a formic acid leading to the formation of *N,N*-dimethyl carbamothioic acid. The yellow, black, white, blue, and red colors represent sulfur, carbon, hydrogen, nitrogen, and oxygen atoms, respectively.

Similarly, the OCS••DMA (RC3) + H_2O and the OCS••H_2O (RC5) + DMA reaction channels lead to the formation of alternative reaction paths (eqns. 8 and 9).

$$OCS••DMA + H_2O \rightarrow HO\text{-}C(=S)N(CH_3)_2 + H_2O \quad (8)$$

$$OCS••H_2O + DMA \rightarrow HO\text{-}C(=S)N(CH_3)_2 + H_2O \quad (9)$$

The PES profiles and the corresponding energies of all the minima on the PES are presented in Figure 6. The OCS••DMA (RC3) + H_2O and OCS••H_2O (RC5) + DMA reaction channels proceed to form an alternative pre-reactant complex (PRC10), which then leads to a transition state (TS16) with a barrier height of ~12.3 kcal mol^{-1} above that of the starting reactants. The structure of TS16 suggests that the DMA addition to OCS is followed by transfer of the H-atom to the O-atom of OCS with the assistance of a water molecule. The reaction continues to form PC10, which then undergoes decomposition to form P_6 + H_2O as products. Therefore, when a single water molecule is involved in the OCS + DMA reaction, which proceeds through an H-atom shift to the S-atom of OCS, the barrier height is reduced by ~12.9 kcal mol^{-1}, whereas in the case of H-atom transfer to the O-atom of OCS, it is reduced by ~20 kcal mol^{-1} compared to the value for the uncatalyzed OCS + DMA reaction.

3.1.7. The reaction of OCS with $(CH_3)_2NH$ assisted by a single HC(O)OH molecule:

Calculations were also performed on DMA + OCS assisted by a FA, and leading to the formation of *N,N*-dimethyl carbamothioic acid. The PES profiles are shown in Figure 8. The M06-2X/aug-cc-pVTZ optimized geometries for the OCS + DMA + FA reaction are shown in Figure 7. Like the aforementioned OCS + DMA + H_2O reaction, the present OCS + DMA + FA reaction also proceeds via bimolecular collision pathways. Three possible elementary reactions defined by the three possible dimer complexes OCS••DMA, OCS••FA, and DMA••FA are presented in eqs. (10 – (12)

$$OCS\bullet\bullet DMA + FA \rightarrow HS\text{-}C(=O)N(CH_3)_2 + FA \quad (10)$$

$$OCS\bullet\bullet FA + DMA \rightarrow HS\text{-}C(=O)N(CH_3)_2 + FA \quad (11)$$

$$DMA\bullet\bullet FA + OCS \rightarrow HS\text{-}C(=O)N(CH_3)_2 + FA \quad (12)$$

The structures of OCS••DMA (RC3), OCS••FA (RC7), and DMA••FA (RC8) are shown in Figure 7. We did not take into account the DMA••FA + OCS reaction channel (eqn. 12) because the structure of DMA••FA shows that the H-atom of FA blocks the DMA nitrogen site by forming a hydrogen bond, and it is therefore not available to attack the C-atom of OCS. The binding energies of RC3 and RC7 were both calculated to be ~2.9 kcal mol^{-1} at the CCSD(T)//M06-2X level of theory. The OCS••DMA (RC3) and OCS••FA (RC7) dimer complexes further react with the other remaining reactant molecule through OCS••DMA + FA and OCS••FA + DMA (eqns. 10 and 11). This can be seen from the PES profile for the OCS + DMA + FA reaction entrance channels in Figure 8. These OCS••DMA + FA and OCS••FA + DMA reaction paths proceed further to form a pre-reactant complex (PRC11) with a binding energy of ~9.4 kcal mol^{-1}. The formed PRC11 leads to the formation of TS17 with a barrier height that is -4.2 kcal mol^{-1} below that of the separated OCS + DMA + FA reactants (see Figure 8). The structure of TS17 suggests that the addition of DMA to the C-atom of OCS followed by H-atom transfer from the -NH moiety of DMA to the S-atom of OCS is assisted by a FA molecule (see Figure 7). The reaction further progresses via the formation of a post reactive complex (PC11) and then on to the formation of P_3 + FA as separated products.

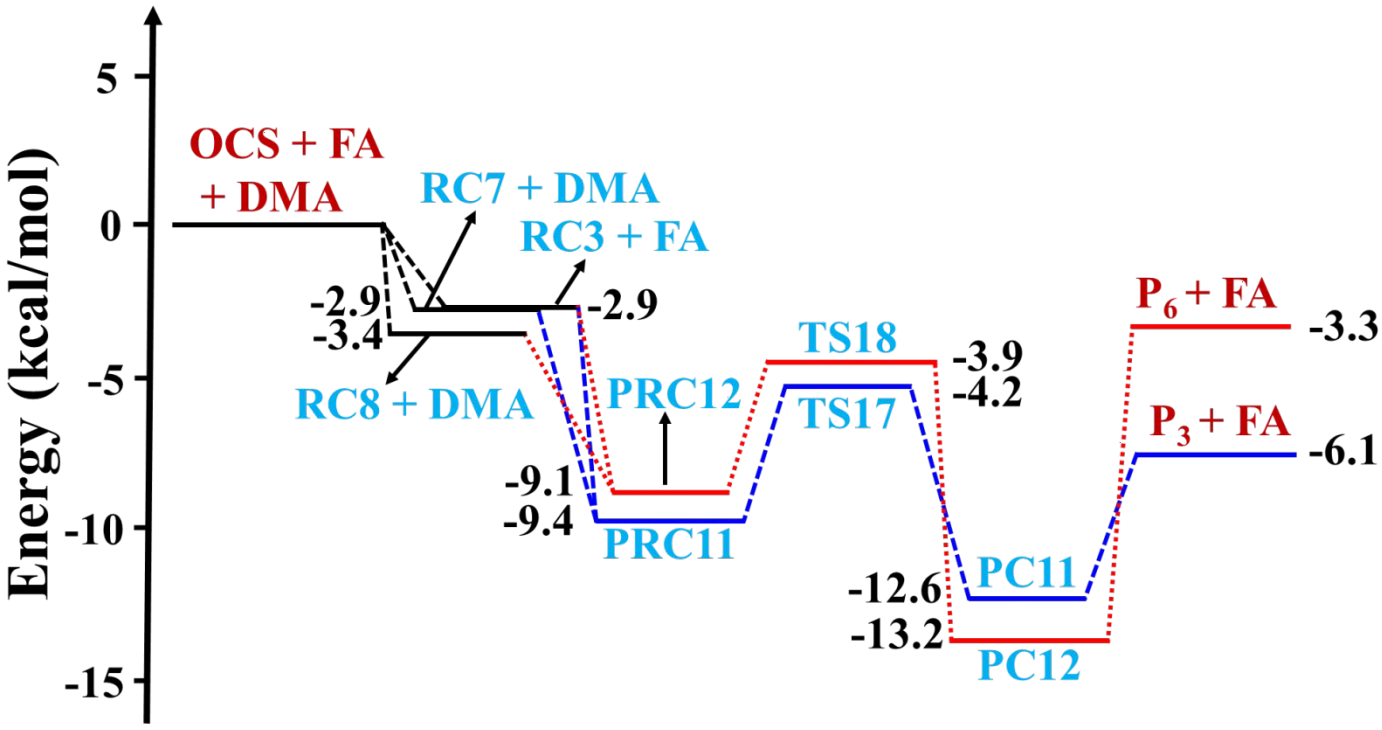

Figure 8. The CCSD(T)/aug-cc-pVTZ//M0-62X/aug-cc-pVTZ calculated potential energy surface diagram for the addition of dimethyl amine to OCS followed by migration of the H-atom to either the S-atom (indicated using blue lines) or O-atom (indicated with red lines) of OCS catalyzed by a formic acid to form *N,N*-dimethyl carbamothioic acid. The symbols RC3, RC7 and RC8; PRC11 and PRC12; TS17 and TS18; PC11 and PC12; TS17 and TS18; and P_3 and P_6 refer to the dimer complexes, the pre-reactant complexes, the transition states, the post reactive complexes, and the *N,N*-dimethyl carbamothioic acid products, respectively.

We next performed calculations on the addition of DMA to OCS, followed by transfer of the H-atom from the -NH group to the O-atom of OCS, assisted by a FA. The possible bimolecular reaction channels are given in eqns. 13 and 14.

$$OCS{\bullet\bullet}DMA + FA \rightarrow HO\text{-}C(=S)N(CH_3)_2 + FA \quad (13)$$

$$OCS{\bullet\bullet}FA + DMA \rightarrow HO\text{-}C(=S)N(CH_3)_2 + FA \quad (14)$$

The PES profile for these two reaction paths are also shown in Figure 8. The OCS + DMA + FA reaction first forms OCS••DMA (RC3) and OCS••FA (RC8) dimer complexes. RC3 and RC8 further react with another species via OCS••DMA + FA and OCS••FA + DMA leading to the formation of TS18 with a barrier height of ~-3.9 kcal mol^{-1} below that of the separated reactants. The formed TS18 is located between the corresponding pre-reactant complex (PRC12) and post-reactive complex (PC12), and finally leads to the formation of P_6 + FA as products. The barrier heights in Figure 8 suggest that the OCS + DMA + FA reaction leading to the formation of TS17 and then to product (P_3) is energetically more favorable compared to the formation of the alternative TS18 to form product (P_6).

The CCSD(T)//M06-2X level calculated barrier heights for the addition of three different amine molecules with OCS without catalysis, and assisted by a H_2O or a FA molecule were shown in Figures 1-5, and 8. We observed the trend that the barrier heights for the reactions in eqns. 1-4 decrease along the series NH_3, MA, and DMA. It is also apparent from the figures that this trend aligns with the increase in the nucleophilic character of the reactants along the series for the reactions without catalysis and with catalysis by a H_2O and a FA molecule. In addition, the transition states for the unassisted reaction, and for the reactions assisted by a H_2O and a FA, involve four, six, and eight membered ring-like structures, respectively. Similar TS structures were reported for the reaction of isocyanic acid (HNCO) with DMA catalyzed by a single H_2O molecule.[43] The present work shows that in the case of FA as a catalyst, the reaction barrier associated with carbamothioic S- or O acid formation can be decreased by varying the R group on the amine nitrogen (see eqns. 3 and 4). In the case of NH_3, the barrier height was found to be 9.8 and 9.0 kcal mol^{-1}. For methylamine, the barrier energy reduces to 1.0 and -0.2 kcal mol^{-1}, and in the case of dimethylamine, the barrier energies drop to -4.2 and -3.9 kcal mol^{-1} relative to those of

the starting reactants, respectively. Therefore, by varying the R group on the nitrogen, the barrier height changes over a range of ~14, ~13 kcal mol^{-1}, respectively.

The transition states (TS1-TS18) in the present work clearly show that the C—N bond length (~1.50 ±0.01 Å) is very close to the normal C—N bond length of ~1.47 Å. This suggests the possibility that the mechanism for the OCS + amine reaction may proceed in two steps (i.e. C—N bond formation followed by hydrogen transfer). Thus, we performed optimization of the transition states for the addition of the three different amines to OCS, proceeding to the formation of the C—N bond both without catalysis and in the presence of water and formic acid at the M06-2X/aug-cc-pVTZ level. Although we searched extensively, we did not find a transition state associated with the C—N bond formation step for any of the possible OCS + amine reactions at the present level of theory. Therefore, we conclude that the OCS + amine reaction mainly proceeds via single step mechanism as suggested in this work. As an example, the IRC plots obtained at the M06-2X/aug-cc-pVTZ level for the addition of DMA to OCS followed by transfer of the H-atom to either the S-atom or O-atom of OCS without catalysis and in the presence of water and FA are shown in Figure S3-S8, respectively. For the OCS + DMA reaction shown in Figure S3, the structures presented from left to right in the IRC plot indicate that the reactant molecules OCS and DMA initially approach each other by forming the C—N bond, and then the H-atom of DMA starts to migrate to the S-atom of OCS before reaching the transition state. After passing the transition state, the H-atom of DMA finally forms a bond with the S-atom of OCS (see Figure S3). The structures in the IRC plot for the OCS + DMA + H_2O reaction (see Figure S4) suggest that OCS and DMA primarily approach each other by forming the C—N bond and then hydrogen atom transfer occurs at the DMA to the O-atom of H_2O before reaching the transition state. After passing the transition state, the H-atom of DMA forms a bond with the O-atom of H_2O and simultaneously,

the H-atom of H_2O migrates to the S-atom of OCS (see Figure S4). Similarly, in the case of the OCS + DMA + FA reaction, the OCS and DMA approach one another before reaching the transition state. Then the reaction proceeds after passing the transition state through the H-atom of DMA, and forms a single bond with the O-atom of FA with simultaneous transfer of the H-atom of FA to the S-atom of OCS (see Figure S5). Similar mechanism was observed for the addition of DMA to OCS followed by transfer of the H-atom to the O-atom of OCS without catalysis and presence of water and FA (see Figures S6-S8). In addition, we have also found similar mechanism for the OCS + NH_3, OCS + NH_3 + H_2O, OCS + NH_3 + FA, OCS + MA, and OCS + MA + FA reactions, respectively. The results for all these reaction mechanisms indicate that the displacements of heavy atoms and H-atom transfers occur concertedly throughout the reaction. Therefore, the present analysis suggests that the OCS + amine reaction proceeds via C—N bond formation followed by hydrogen transfer in a single step mechanism.

The complexes formed in the OCS + NH_3 reaction in the presence of water and formaldehyde were optimized at M06-2X/aug-cc-pVTZ level with Grimme's third generation dispersion correction (M06-2X-D3).[73] The energies of the complexes were also refined by performing CCSD(T)/aug-cc-pVTZ on the M06-2X-D3 level optimized geometries. The comparison of energies for the various complexes involved in the OCS + NH_3 reaction assisted by a water and formic acid calculated at the M06-2X, M06-2X-D3 and their corresponding CCSD(T)/aug-cc-pVTZ levels are displayed in Table S6. All the energies of the stationary points displayed in Table S6 were calculated relative to the separated starting reactants. The data from the table clearly suggests that the M06-2X-D3 level energies of the complexes varied by ~0.1 kcal mol^{-1} compared to the values at the M06-2X level. We also observed no change in the energies for the complexes at the CCSD(T)//M06-2X-D3 level compared to the values at the CCSD(T)//M06-

2X level. Therefore, the empirical dispersion correction calculations were not performed for the OCS + MA + H_2O, OCS + MA + FA, OCS + DMA + H_2O, and OCS + DMA + FA reactions, respectively.

The energies of the pre-reactive complexes (PRC1 and PRC2) involved in the OCS + NH_3 + H_2O reaction at the CCSD(T)//M06-2X level were found to be 11.3 and -5.8 kcal mol^{-1} respectively (see Table S6 and Figures 2). In the case of the OCS + NH_3 + FA reaction, the energies of the pre-reactive complexes (PRC3 and PRC4) calculated at the CCSD(T)//M06-2X level were found to be 5.4 and 5.3 kcal mol^{-1} above that of the starting reactants (see Table S6 and Figure 3). We note that the calculated energies of PRC1, PRC3, and PRC4 that are associated with the OCS + NH_3 + H_2O and OCS + NH_3 + FA reactions indicate that they are located above the stating reactants (see Table S6 and Figures 2-3). We also observed a similar trend in the energies of the pre-reactive complexes, which are located above the separated reactants for the analogous reaction (HNCO + NH_3 + H_2O) reported in the literature.[43] The energies of the post-reactive complexes (PC1, PC2, PC3, and PC4) associated with the OCS + NH_3 + H_2O and OCS + NH_3 + FA reactions calculated at the CCSD(T)//M06-2X level were determined to be -2.2, 5.3, -4.8, and 2.0 kcal mol^{-1}, respectively. Similar trends in energies were observed for all the stationary points in Table S6 for the OCS + NH_3 + H_2O and OCS + NH_3 + FA reactions at various levels of theory, such as the M06-2X, M06-2X-D3, and CCSD(T)//M06-2X-D3 levels.

3.2. Theoretical Kinetic Analysis:

The OCS + NH_3 and OCS + MA reactions in the absence of catalysts and presence of a single molecule of H_2O or FA exhibit very high barriers (see Figures 1a-b-5). Therefore, these

reactions are energetically not feasible under normal atmospheric conditions. The OCS + DMA reaction catalyzed by a single FA molecule shows negative barrier heights for the formation of *N,N*-dimethyl-carbamothioic acid (see Figure 8). Therefore, rate coefficient calculations for the OCS + DMA reaction for both the absence of catalysis and the presence of single H_2O and FA molecules were calculated to determine the quantitative effect of these two catalysts, in comparison with the absence of catalysis in the atmospheric removal of OCS the presence of DMA. In doing so, we followed previously published procedures for computing the reaction kinetics.[43, 55, 56] The reaction scheme for OCS + DMA in the absence of a catalyst can be represented by eq. 15:

$$\mathrm{OCS + DMA} \underset{k_{-1}}{\overset{k_1}{\rightleftharpoons}} \mathrm{OCS\bullet\bullet DMA} \xrightarrow{k_2} \mathrm{Products} \qquad (15)$$

The reaction between the two reactant species OCS and DMA primarily forms a two-body OCS••DMA complex (eqn.15) which undergoes unimolecular isomerization through a TS leading to the formation of final products. The symbols k_1 and k_{-1} represent the forward and reverse rate coefficients for the OCS + DMA reactions to form a OCS••DMA complex. The symbol k_2 represents the unimolecular rate coefficient for product formation from the OCS••DMA complex via a well-defined TS. We assumed that the two-body complex is in equilibrium with the reactants, and that the rate of the uncatalyzed reaction under pre-equilibrium conditions can be approximated by:

$$\mathrm{Rate} = k[\mathrm{OCS}][\mathrm{DMA}] \qquad (16)$$

In eqn. 16, k represents the rate coefficient (in cm^3 $molecule^{-1}$ s^{-1}) for the uncatalyzed OCS + DMA reaction; $k = K_{eq1}k_2$; and the equilibrium constant K_{eq1} represents the formation of the

OCS••DMA complex from the OCS and DMA reactants. Using eqn. 15, K_{eq1} can defined as K_{eq1}= $\frac{k_1}{k_{-1}}$.

As an example, the OCS••DMA complex primarily reacts with a catalyst X (X = H_2O or FA) to form a OCS••DMA••X pre-reactant complex, which then undergoes intramolecular isomerization to form a post-reactive complex (PC) via a TS. The reaction scheme for the OCS••DMA + X (X = H_2O or FA) can be represented by eqn.17

$$\text{OCS}\bullet\bullet\text{DMA} + \text{X} \underset{k_{-3}}{\overset{k_3}{\rightleftharpoons}} \text{OCS}\bullet\bullet\text{DMA}\bullet\bullet\text{X} \xrightarrow{k_4} \text{PC} \qquad (17)$$

Similar to the uncatalyzed OCS + DMA reaction mechanism given in eqn. 15, the pre-reactant complex (OCS••DMA••X) is assumed to be in equilibrium with the OCS••DMA and X (X=H_2O or FA) reactants. The symbols k_3 and k_{-3} represent the forward and reverse rate coefficients for the OCS••DMA + X reaction to form the OCS••DMA••X complex. The symbol k_4 represents the unimolecular rate coefficient for the reaction step involving conversion of OCS••DMA••X complex to the PC via a well-defined TS. The rate of the OCS••DMA + X reaction under pre-equilibrium conditions is given in eqn. 18

$$\text{Rate} = k_X[\text{OCS}\bullet\bullet\text{DMA}][\text{X}] \qquad (18)$$

In eqn. 18, k_X represents the rate coefficient for the reaction of OCS••DMA + X (X= H_2O or FA) $k_X = K_{eqX}k_4$; and the equilibrium constant K_{eqX} represents the formation of the OCS••DMA••X complex from the isolated reactants. Using eqn. 17, K_{eqX} can be defined as: $K_{eqX} = \frac{k_3}{k_{-3}}$. The unimolecular rate coefficients (k_2 and k_4) were computed with Polyrate (2016) kinetic code[74] by employing canonical variational transition state theory,[58, 59] and tunneling contributions were calculated with the small curvature tunneling[60] method using eqn. 19

$$k_2, (k_4)(\mathrm{CVT/SCT}) = \kappa^{\mathrm{SCT}} \frac{k_\mathrm{B} \mathrm{T} \mathrm{Q}_{\mathrm{GT}}(s^*)}{h \quad \mathrm{Q}_{\mathrm{RC}}} e^{\frac{-V(S^*)}{k_B T}} \qquad (19)$$

In eqn. 19, κ^{SCT} is the small curvature tunneling factor; s* is the value of the reaction coordinate at the free energy maximum along the reaction path; V(s*) is the potential energy at the barrier maximum; k_B is Boltzmann's constant; h is Planck's constant; T is the temperature in Kelvin; and Q_{RC} and Q_{GT}(s*) are the partition functions of the pre-reactant complex and transition state, respectively.

The equilibrium constants (K_{eq1} and K_{eqX}) were calculated using eqns. 20 and 21:

$$K_{\mathrm{eq1}} = \frac{Q_{\mathrm{OCS\bullet\bullet DMA}}}{Q_{\mathrm{OCS}}\, Q_{\mathrm{DMA}}} \exp\left(- \frac{E_{\mathrm{OCS\bullet\bullet DMA}} - E_{\mathrm{OCS}} - E_{\mathrm{DMA}}}{k_B T} \right) \qquad (20)$$

$$K_{\mathrm{eqX}} = \frac{Q_{\mathrm{RC_X}}}{Q_{\mathrm{OCS\bullet\bullet DMA}} Q_{\mathrm{X}}} \exp\left(- \frac{E_{\mathrm{RC_X}} - E_{\mathrm{OCS\bullet\bullet DMA}} - E_{\mathrm{X}}}{k_B T} \right) \qquad (21)$$

In eqn 20, the partition function of a OCS••DMA dimer complex formed from the OCS and DMA reactants are represented by the symbols $Q_{\mathrm{OCS\bullet\bullet DMA}}$, Q_{OCS}, and Q_{DMA}, respectively. $E_{\mathrm{OCS\bullet\bullet DMA}}$, E_{OCS}, and E_{DMA} are the zero-point corrected total energies of the OCS••DMA dimer complex, OCS, and DMA reactants respectively. Similarly, using eqn 21, the partition function of RC (RC_X) derived from the respective OCS••DMA dimer complex and the other reactant X (X = H_2O or FA) are represented by the symbols $Q_{\mathrm{RC_X}}$, $Q_{\mathrm{OCS\bullet\bullet DMA}}$, and Q_{X}, respectively. $E_{\mathrm{RC_X}}$, $E_{\mathrm{OCS\bullet\bullet DMA}}$, and E_{X} represent the zero-point corrected total energies of the respective RC and reactant species.

The pre-reactive complexes such as OCS••DMA••H_2O and OCS••DMA••FA are formed from their corresponding reactants (OCS, DMA, H_2O, FA) as shown in the first step of eqn.17. Various studies have demonstrated that the presence of pre-reactive complexes has a significant

effect on the progress of the reaction.[75-77] This can occur because the formed complexes can spatially direct the site of the reaction by either steric hindrance or through provision of a pre-reactive potential energy well. Therefore, complex formation can have a major impact on the rate coefficients.

The bimolecular rate coefficients (in cm^3 $molecule^{-1}$ s^{-1}) for the OCS + DMA uncatalyzed reaction (eqns. 1 and 2) were calculated using the expressions: $k_{TS3} = K_{eq1}k_2$ and $k_{TS6} = K_{eq1}k_6$, respectively. In these expressions, the equilibrium constant K_{eq1} is associated with the formation of the OCS••DMA complex from the OCS, DMA reactants. The calculated temperature dependent unimolecular rate coefficients (k_2 and k_6), equilibrium constant (K_{eq1}), bimolecular rate coefficients (k_{TS3} and k_{TS6}), and tunneling contributions in the temperature range 200 – 300 K are provided in Tables S7 and S9 and Table 1. The bimolecular rate coefficient data in Table 1 suggest that in the studied temperature range, addition of DMA to OCS followed by H-atom transfer to the S-atom of OCS through TS3 is ~10^5-10^7 times faster than the addition of DMA to OCS that is followed by H-atom transfer to the O-atom of OCS through TS6. This difference is mainly because the barrier height for TS3 is ~7.8 kcal mol^{-1} lower than that for TS6. The calculated rate coefficients at 300 K for the OCS + DMA reaction via TS3 and TS6 were found be $k_{TS3} = 5.28 \times 10^{-31}$ and $k_{TS6} = 4.20 \times 10^{-36}$ cm^3 $molecule^{-1}$ s^{-1}. The small curvature tunneling contributions (κ_{TS3}^{SCT} and κ_{TS6}^{SCT}) given in Table 1 show that the magnitude of the tunneling factor is significant, as it varies between ~1-4 orders for TS3 and ~2-7 orders for TS6 in the studied temperature range.

Table 1. The calculated rate coefficients (k_{TS3} and k_{TS6} in cm^3 $molecule^{-1}$ s^{-1}) and the corresponding tunneling factors (κ) for the OCS + DMA uncatalyzed reaction to form *N,N*-dimethyl carbamothioic acid in the temperatures between 200 and 300 K.

T(K)	k_{TS3}	κ_{TS3}^{SCT}	k_{TS6}	κ_{TS6}^{SCT}
200	1.61×10^{-36}	9.39×10^{4}	5.62×10^{-43}	1.42×10^{7}
210	7.64×10^{-36}	2.41×10^{4}	3.32×10^{-42}	1.81×10^{6}
220	3.37×10^{-35}	7.50×10^{3}	2.22×10^{-41}	3.67×10^{5}
230	1.36×10^{-34}	2.70×10^{3}	1.35×10^{-40}	9.27×10^{4}
240	5.21×10^{-34}	1.11×10^{3}	7.50×10^{-40}	2.75×10^{4}
250	1.87×10^{-33}	5.15×10^{2}	3.79×10^{-39}	9.44×10^{3}
260	6.35×10^{-33}	2.63×10^{2}	1.77×10^{-38}	3.65×10^{3}
270	2.05×10^{-32}	1.47×10^{2}	7.66×10^{-38}	1.58×10^{3}
280	6.33×10^{-32}	8.83×10^{1}	3.09×10^{-37}	7.46×10^{2}
290	1.86×10^{-31}	5.67×10^{1}	1.17×10^{-36}	3.84×10^{2}
298	4.37×10^{-31}	4.12×10^{1}	3.33×10^{-36}	2.36×10^{2}
300	5.28×10^{-31}	3.86×10^{1}	4.20×10^{-36}	2.13×10^{2}

The rate coefficients (in cm^3 $molecule^{-1}$ s^{-1}) for the OCS••DMA + H_2O (k_5) and OCS••H_2O + DMA (k_6) reaction paths that proceed via H-atom transfer to the S-atom of OCS, and alternatively, via H-atom transfer to the O-atom of OCS for the OCS••DMA + H_2O (k_8), and OCS••H_2O + DMA (k_9) reactions, respectively were calculated using the expressions: $k_5 = K_{eq2}k_7$, $k_6 = K_{eq3}k_7$, $k_8 = K_{eq4}k_{15}$, and $k_9 = K_{eq5}k_{15}$, respectively. In these expressions, k_7 and k_{15} represent the unimolecular rate coefficients, and the equilibrium constants (K_{eq2}, K_{eq3}, K_{eq4}, and K_{eq5}) are associated with the PRC9 and PRC10 formation steps of the OCS••DMA + H_2O, and OCS••H_2O + DMA reactants. The calculated equilibrium constants, unimolecular and corresponding bimolecular rate coefficients for these dimer reactions were determined in the temperatures between 200 and 300 K and the values are displayed in Table S8, Table S9 and Table 2. The data in Table 2 suggest that at 300 K, the rate coefficients for the OCS••DMA + H_2O (k_5) and OCS••H_2O + DMA (k_6) reactions for the addition of DMA followed by H-atom transfer to the S-atom of OCS (TS15) were found to be 5.16×10^{-25} cm^3 $molecule^{-1}$ s^{-1} and 2.02×10^{-25} cm^3

molecule^{-1} s^{-1}, respectively. On the other hand, for the alternative pathways involving OCS••DMA + H_2O (k_8), and OCS••H_2O + DMA (k_9) with H-atom transfer to the O-atom of OCS (TS16), they were found to be 1.22×10^{-26} cm^3 molecule^{-1} s^{-1} and 5.18×10^{-27} cm^3 molecule^{-1} s^{-1} respectively at the same temperature. The data also show that at 300 K, the OCS••DMA + H_2O (k_5) and OCS••H_2O + DMA (k_6) rate coefficients that proceed via TS15 are ~1 order of magnitude higher than the values observed for the OCS••DMA + H_2O (k_8), and OCS••H_2O + DMA (k_9) reactions that occur via TS16.

Similarly, rate coefficients for the OCS••DMA + FA (k_{10}) and OCS••FA + DMA (k_{11}) reaction channels that proceed via H-atom transfer to the S-atom of OCS were calculated using the expressions: $k_{10} = K_{eq6}k_{16}$, and $k_{11} = K_{eq7}k_{16}$, respectively. The rate coefficients for the alternative pathways for the OCS••DMA + FA (k_{13}) and OCS••FA + DMA (k_{14}) reactions that proceed through H-atom transfer to the O-atom of OCS, were calculated using equations: $k_{13} = K_{eq8}k_{17}$ and $k_{14} = K_{eq9}k_{17}$. In these expressions, k_{16} and k_{17} refer to the unimolecular rate coefficients, and the equilibrium constants K_{eq6}, K_{eq7}, K_{eq8}, and K_{eq9} are associated with PRC11 and PRC12 formation steps from the two possible OCS••DMA + FA, and OCS••FA + DMA dimer reaction pathways. The estimated equilibrium constants, unimolecular and bimolecular rate coefficients for these reactions were also provided in Table S8, Table S9 and Table 2.

Table 2. The calculated bimolecular rate coefficients (in cm^3 $molecule^{-1}$ s^{-1}) for the OCS••DMA + H_2O (k_5), OCS••H_2O + DMA (k_6), OCS••DMA + FA (k_{10}), and OCS••FA + DMA (k_{11}) reaction paths that proceed via H-atom transfer to the S-atom of OCS, and the OCS••DMA + H_2O (k_8), OCS••H_2O + DMA (k_9), OCS••DMA + FA (k_{13}), and OCS••FA + DMA (k_{14}) reaction paths that proceed via H-atom transfer to the O-atom of OCS, respectively to form *N,N*-dimethyl carbamothioic acid.

T(K)	k_5	k_6	k_8	k_9	k_{10}	k_{11}	k_{13}	k_{14}
200	1.15×10^{-27}	1.83×10^{-27}	2.40×10^{-30}	3.58×10^{-30}	2.98×10^{-15}	6.50×10^{-16}	7.06×10^{-16}	1.35×10^{-16}
210	2.54×10^{-27}	3.29×10^{-27}	7.65×10^{-30}	9.53×10^{-30}	2.04×10^{-15}	4.39×10^{-16}	4.99×10^{-16}	9.97×10^{-17}
220	5.30×10^{-27}	5.75×10^{-27}	2.23×10^{-29}	2.37×10^{-29}	1.45×10^{-15}	3.11×10^{-16}	3.67×10^{-16}	7.64×10^{-17}
230	1.06×10^{-26}	9.67×10^{-26}	5.99×10^{-29}	5.46×10^{-29}	1.08×10^{-15}	2.26×10^{-16}	2.79×10^{-16}	5.99×10^{-17}
240	2.03×10^{-26}	1.59×10^{-26}	1.50×10^{-28}	1.19×10^{-28}	8.23×10^{-16}	1.71×10^{-16}	2.18×10^{-16}	4.84×10^{-17}
250	3.74×10^{-26}	2.56×10^{-26}	3.56×10^{-28}	2.49×10^{-28}	6.47×10^{-16}	1.33×10^{-16}	1.75×10^{-16}	4.01×10^{-17}
260	6.69×10^{-26}	4.02×10^{-26}	7.91×10^{-28}	4.93×10^{-28}	5.21×10^{-16}	1.06×10^{-16}	1.44×10^{-16}	3.39×10^{-17}
270	1.16×10^{-25}	6.19×10^{-26}	1.67×10^{-27}	9.37×10^{-28}	4.29×10^{-16}	8.67×10^{-17}	1.21×10^{-16}	2.92×10^{-17}
280	1.95×10^{-25}	9.32×10^{-26}	3.38×10^{-27}	1.72×10^{-27}	3.58×10^{-16}	7.19×10^{-17}	1.03×10^{-16}	2.54×10^{-17}
290	3.22×10^{-25}	1.38×10^{-25}	6.57×10^{-27}	3.04×10^{-27}	3.05×10^{-16}	6.08×10^{-17}	8.88×10^{-17}	2.25×10^{-17}
298	4.74×10^{-25}	1.89×10^{-25}	1.09×10^{-26}	4.71×10^{-27}	2.71×10^{-16}	5.36×10^{-17}	7.96×10^{-17}	2.06×10^{-17}
300	5.16×10^{-25}	2.02×10^{-25}	1.22×10^{-26}	5.18×10^{-27}	2.63×10^{-16}	5.20×10^{-17}	7.76×10^{-17}	2.01×10^{-17}

The data in Table 2 show that at 300 K, the rate coefficients for the OCS••DMA + FA (k_{10}) and OCS••FA + DMA (k_{11}) reactions proceeding via TS17 were 2.63×10^{-16} cm^3 molecule^{-1} s^{-1} and 5.20×10^{-17} cm^3 molecule^{-1} s^{-1} respectively. For the alternative pathways OCS••DMA + FA (k_{13}), and OCS••FA + DMA (k_{14}) which proceed via TS18, the rate coefficients were 7.76×10^{-17} cm^3 molecule^{-1} s^{-1} and 2.01×10^{-17} cm^3 molecule^{-1} s^{-1} respectively at the same temperature. The data also show that the rate coefficients for the OCS••DMA + FA (k_{10}) and OCS••FA + DMA (k_{11}) reactions that proceed via TS17 are ~3 times larger than the values for the OCS••DMA + FA (k_{13}) and OCS••FA + DMA (k_{14}) reactions that occur via TS18 in the studied temperature range.

The effectiveness of a catalyst on a specific reaction in the atmosphere depends not only on the rate coefficient, but also on the rate of the reaction. Therefore, it is very important to compare the rates of reactions. Information such as the rate coefficient and the concentrations of the participating reactants allow comparisons to made of the impacts of different catalysts on a specific reaction. For this reason, we compared the rates of the reactions involving OCS + DMA both without catalysis and in the presence of single H_2O and FA molecules. The rates of the OCS + DMA reaction, proceeding via TS3 and TS6 are given in eqns. 22 and 23.

$$\text{rate} = k_{TS3}[\text{OCS}][\text{DMA}] = k_{TS3}^{\text{eff}}[\text{OCS}] \quad (22)$$

$$\text{rate} = k_{TS6}[\text{OCS}][\text{DMA}] = k_{TS6}^{\text{eff}}[\text{OCS}] \quad (23)$$

In eqns. 22 and 23, k_{TS3}^{eff} and k_{TS6}^{eff} represent effective first order rate coefficients for the uncatalyzed reactions of OCS + DMA, and can be defined as $k_{TS3}^{\text{eff}} = k_{TS3}[\text{DMA}]$ and $k_{TS6}^{\text{eff}} = k_{TS6}[\text{DMA}]$. The rate for the OCS••DMA + H_2O and OCS••H_2O + DMA reactions via TS15 and TS16 can be written in terms of the bimolecular rate coefficients and the corresponding reactant and dimer concentrations using eqns. 24-27.

$$\text{rate} = k_5[\text{OCS}\bullet\bullet\text{DMA}][H_2O] = k_5 Keq1[\text{OCS}][\text{DMA}][H_2O] = k_5^{\text{eff}}[\text{OCS}] \quad (24)$$

$$\text{rate} = k_6[\text{OCS}\bullet\bullet H_2O][\text{DMA}] = k_6 Keq10[\text{OCS}][\text{DMA}][H_2O] = k_6^{\text{eff}}[\text{OCS}] \quad (25)$$

$$\text{rate} = k_8[\text{OCS}\bullet\bullet\text{DMA}][H_2O] = k_8 Keq1[\text{OCS}][\text{DMA}][H_2O] = k_8^{\text{eff}}[\text{OCS}] \quad (26)$$

$$\text{rate} = k_9[\text{OCS}\bullet\bullet H_2O][\text{DMA}] = k_9 Keq11[\text{OCS}][\text{DMA}][H_2O] = k_9^{\text{eff}}[\text{OCS}] \quad (27)$$

In eqns. 24-27, k_5^{eff}, k_6^{eff}, k_8^{eff}, and k_9^{eff} represent the effective first order rate coefficients for the removal of OCS through these reactions. They were defined as: $k_5^{\text{eff}} = k_5 Keq1[\text{DMA}][H_2O]$, $k_6^{\text{eff}} = k_6 Keq10[\text{DMA}][H_2O]$, $k_8^{\text{eff}} = k_8 Keq1[\text{DMA}][H_2O]$, and $k_9^{\text{eff}} = k_9 Keq11[\text{DMA}][H_2O]$. The symbols Keq1, Keq10 and Keq11 represent the equilibrium constants for the formation of the corresponding dimer complexes.

Similarly, the rate for the OCS••DMA + FA and OCS••FA + DMA reactions via TS17 and TS18 were calculated using the corresponding parameters k_{10}^{eff}, k_{10}, and Keq1, with $k_{10}^{\text{eff}} = k_{10} Keq1[\text{DMA}][\text{FA}]$; k_{11}^{eff} , k_{11}, and Keq12 with $k_{11}^{\text{eff}} = k_{11} Keq12[\text{DMA}][\text{FA}]$; k_{13}^{eff} , k_{13}, and Keq1 with $k_{13}^{\text{eff}} = k_{13} Keq1[\text{DMA}][\text{FA}]$; and k_{14}^{eff}, k_{14}, and Keq13 with $k_{14}^{\text{eff}} = k_{14} Keq13[\text{DMA}][\text{FA}]$. The k_{10}^{eff}, k_{11}^{eff}, k_{13}^{eff}, and k_{14}^{eff} refer to the effective first order rate coefficients for the reaction of OCS + DMA assisted by a single FA molecule. The symbols Keq1, Keq12, and Keq13 represents the equilibrium constants for the formation of dimer complexes. The equilibrium constants for the various dimer complexes are given in Table S7 of the supporting information. The temperature dependent concentrations of H_2O (assumed to be 10%-100% RH) are displayed in Table S10. Other participating reactants used in this work were as follows: [DMA] = 2.0×10^8 molecules cm^{-3}; and [FA] = 4.4×10^{11} molecules cm^{-3}.[43, 56] In the cases of the OCS + DMA + H_2O and OCS + DMA + FA reactions involving multiple reaction pathways, the total effective rate coefficients (in s^{-1}) for the overall reaction were calculated by summing the individual effective rate coefficients for each branch using the expressions: $k_{\text{TS15}}^{\text{eff}} = k_5^{\text{eff}} + k_6^{\text{eff}}$; $k_{\text{TS16}}^{\text{eff}} = k_8^{\text{eff}} + k_9^{\text{eff}}$; $k_{\text{TS17}}^{\text{eff}} =$

$k_{10}^{\mathrm{eff}} + k_{11}^{\mathrm{eff}}$; and $k_{\mathrm{TS18}}^{\mathrm{eff}} = k_{13}^{\mathrm{eff}} + k_{14}^{\mathrm{eff}}$, where the symbols $k_{\mathrm{TS15}}^{\mathrm{eff}}$ and $k_{\mathrm{TS16}}^{\mathrm{eff}}$ represent the total rate coefficients for the OCS + DMA + H_2O reaction involving H-atom transfer to either the S-atom or O-atom of OCS, and $k_{\mathrm{TS17}}^{\mathrm{eff}}$ and $k_{\mathrm{TS18}}^{\mathrm{eff}}$ represent the total rate coefficient for the OCS + DMA + FA reaction involving H-atom transfer to either the S-atom or O-atom of OCS. The calculated effective first order rate coefficient values for the OCS + DMA, OCS + DMA + H_2O, and OCS + DMA + FA reactions involving two possible H-atom transfer reaction paths are given in Tables S10 and S11.

To better understand the impact of temperature, the effective first order rate coefficients were plotted against temperature, and the results for the two possible H-atom transfers involving OCS + DMA in the absence and presence of H_2O and FA single molecules are presented in Figure 9. It is clear from the plot that the effective rate coefficients for the two possible H-atom transfers involving the OCS + DMA, and OCS + DMA + H_2O reaction pathways increase with temperature, whereas the effective rate coefficient values for the OCS + DMA + FA channels decrease with temperature. This difference in rate coefficient trends occurs because while the OCS + DMA reaction (via TS3 and TS6), and the OCS + DMA + H_2O reactions (via TS15 and TS16) show significant positive barrier heights, the OCS + DMA + FA reactions (via TS17 and TS18) have negative energy barriers. The effective first order rate coefficient data in Table S10 and Figure 9 suggest that for the OCS + DMA + H_2O reaction, H-atom transfer to the S-atom of OCS is ~1 orders of magnitude more dominant than the values for the OCS + DMA reaction in the temperatures between 200 and 300 K. For example, the effective rate coefficients for the OCS + DMA, and OCS + DMA + H_2O reactions at 298 K were calculated to be 8.74×10^{-23} s^{-1}, and 4.51×10^{-22} s^{-1} respectively. The OCS + DMA + FA reaction was ~10^3 – 10^{10} times more dominant compared to the values for the OCS + DMA + H_2O reaction in the studied temperature range.

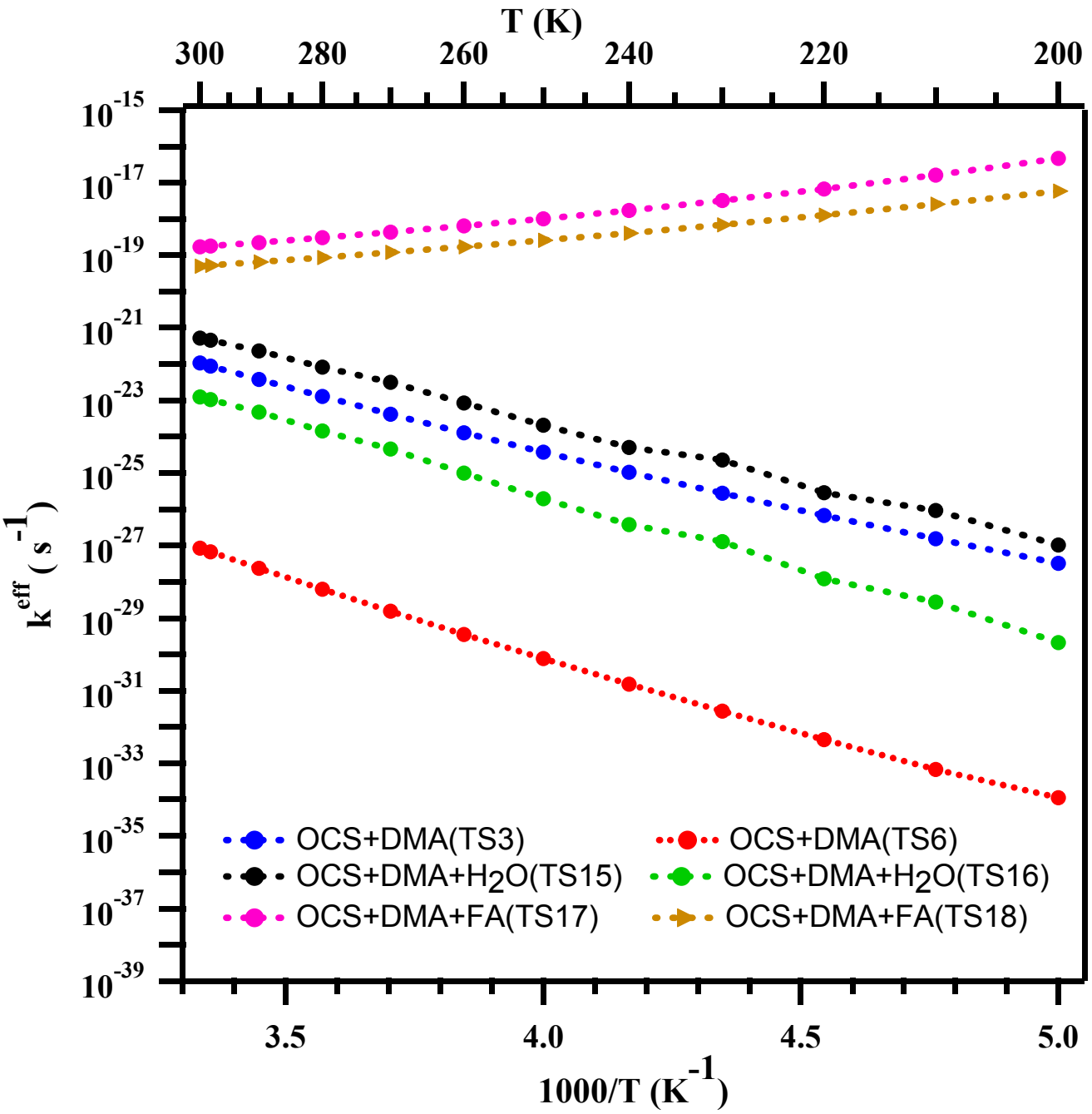

Figure 9. Calculated effective rate coefficient (in s^{-1}) comparison for the reaction of OCS + DMA in the absence of a catalyst, versus assisted by a single water molecule and a formic acid molecule.

At 298 K, the effective rate coefficient for the OCS + DMA + FA reaction was found to be 1.77 × 10^{-19} s^{-1}, which is ~10^3 times larger than the value for the OCS + DMA + H_2O reaction, which had an effective rate coefficient of 4.51 × 10^{-22} s^{-1} at the same temperature. This shows that the rate of the FA catalyzed reaction of OCS + DMA is faster than that for the water catalyzed reaction, even though the concentration of FA is ~3-6 orders of magnitude smaller compared to the concentration of water in the atmosphere. This is mainly due to the fact that the OCS + DMA + FA reaction barrier is ~15.5 kcal mol^{-1} lower than that for the OCS + DMA + H_2O reaction. Similarly, Table S11 and Figure 9 clearly show that the effective rate coefficients for the OCS + DMA + H_2O reaction involving the H-atom shift to the O-atom of OCS is larger by ~10^4-10^5 times the values for the uncatalyzed OCS + DMA reaction in the same temperature range. For example, at 298 K, the effective rate coefficient for the uncatalyzed and water catalyzed OCS + DMA reactions were found to be 6.66 × 10^{-28} s^{-1} and 1.04 × 10^{-23} s^{-1}, respectively. For the OCS + DMA + FA reaction, the effective rate coefficient data suggest that this reaction rate is ~10^3-10^{12} times larger than the values for the OCS + DMA + H_2O reaction in the temperatures within 200 – 300 K. At 298 K, the effective rate coefficient for the OCS + DMA + FA was found to be 5.22 × 10^{-20} s^{-1}, which is ~10^3 times larger than the value for the OCS + DMA + H_2O reaction. This suggests that a single molecule of FA is a more effective catalyst for the OCS + DMA reaction than a single water molecule. Overall, FA was found to be a more effective catalyst than water in catalyzing the OCS + DMA reaction. It was also observed that for the OCS + DMA + FA reaction, H-atom transfer to the S-atom of OCS is more favorable than H-atom transfer to the O-atom of OCS.

We also calculated the rate of atmospheric removal of OCS via the OCS + •OH reaction in order to compare it with the rate of the OCS + DMA + FA reaction. The rate coefficient for the OCS + •OH reaction by various groups at 298 K temperature has been reported to range between

5.7×10^{-14} cm^3 $molecule^{-1}$ s^{-1} – 6.0×10^{-16} cm^3 $molecule^{-1}$ s^{-1}. To get the effective first order rate coefficient for the OCS + •OH reaction, the rate expression can be given by eqn. 28.

$$\text{rate} = k_{OH}[OCS][OH] = k_{OH}^{eff}[OCS] \quad (28)$$

Using eqn.28, the effective rate coefficient can be defined as $k_{OH}^{eff} = k_{OH}[OH]$, where k_{OH} is the reported bimolecular rate coefficient for the OCS + •OH reaction. Using the average atmospheric concentration of [•OH] = 1.0×10^6 molecules cm^{-3} and the reported bimolecular rate coefficients, the effective rate coefficients for the OCS + •OH reactions at 298 K were calculated to be in the range of 5.70×10^{-8} s^{-1} – 6.0×10^{-10} s^{-1}. This suggests that the effective rate coefficients for the OCS + •OH reaction are ~10^{10} times higher than those for the OCS + DMA + FA reaction. Therefore, we concluded that atmospheric removal of OCS through reaction with •OH is more favorable than via the OCS + DMA reaction assisted by either a single water or formic acid molecule. In summary, OCS + DMA + FA, OCS + DMA + H_2O, and OCS + •OH reactions are found to be slow under typical atmospheric conditions, and further studies are required to determine other possible catalysts that can facilitate removal of OCS from the atmosphere.

4. Conclusions:

Atmospheric removal of OCS through reaction with three different amines both in the absence of, and assisted by a single H_2O or formic acid (FA) catalyst, were investigated at the CCSD(T)//M06-2X level of theory. The calculated barrier heights were observed to decrease with increasing methylation on the amine nitrogen atom. Addition of ammonia or methylamine (MA) to OCS assisted by a H_2O or FA and leading to the formation of the corresponding carbamothioic

acids were deemed unfeasible under atmospheric conditions because of high energy barriers. On the other hand, dimethylamine (DMA) + OCS assisted by FA to form *N,N*-dimethyl carbamothioic acid, was found to be an energetically more favorable reaction compared to the uncatalyzed and single H_2O catalyzed reactions. The temperature dependent rate coefficients were computed for the OCS + DMA reactions both without catalysts and in the presence of a single H_2O and a single FA in the temperatures between 200 and 300 K. The results suggest that small curvature tunneling plays an important role in the OCS + DMA reaction when compared to the OCS + DMA reaction assisted by H_2O and FA. The effective rate coefficient results showed that a FA catalyst is more effective for the OCS + DMA reaction by larger than ~10^3 – 10^{10} times for the pathway involving H-atom shift to the S-atom of OCS, and ~10^3-10^{12} times for that involving the H-atom transfer to the O-atom of OCS when compared to the values for the OCS + DMA + H_2O reaction. Even though the OCS + DMA + FA reaction rate is lower compared to the OCS + •OH reaction, it could be a viable path for the atmospheric removal of OCS under night-time forest fire conditions when the OCS and DMA concentrations are high. Thus, although the OCS + DMA + FA reaction was shown be less important in the gas phase based on its lower rate coefficient values, further extensive investigations are required to determine the impact of various other possible catalysts on the OCS + DMA reaction to determine the presence of alternative fates of OCS in the troposphere.

Supporting Information:

Tables S1-S11 presents the optimized geometries of all the stationary points, calculated total electronic energies including zero-point energy corrections, vibrational frequencies and rotational constants, and imaginary frequencies of various TSs as discussed in the text at the M06-2X level,

relative energies of complexes at various levels, temperature dependent unimolecular and effective rate coefficients using CVT/SCT method, equilibrium constants. Figure S1-S2 presents the optimized geometries for the reaction of OCS + NH_3 and OCS + MA, Figure S3-S8 presents the IRC plots for the OCS + DMA, OCS + DMA + H_2O, and OCS + DMA + FA reactions.

Acknowledgements:

The financial support of the National Science Foundation (grant numbers 1310350 and 1710221) to R.A.M is gratefully acknowledged. The authors thank the High-Performance Computing Center at the University at Albany-SUNY for their support.

References:

1. A. R. Bandy, D. C. Thornton, D. L. Scott, M. Lalevic, E. E. Lewin and A. R. Driedger, *J. Atmos. Chem.*, 1992, **14**, 527-534.
2. D. W. T. Griffith, N. B. Jones and W. A. Matthews, *J. Geophys. Res.*, 1998, **103**, 8447-8454.
3. N. Mihalopoulos, J. P. Putaud, B. C. Nguyen and S. Belviso, *J. Atmos. Chem.*, 1991, **13**, 73-82.
4. S. A. Montzka, P. Calvert, B. D. Hall, J. W. Elkins, T. J. Conway, P. P. Tans and C. Sweeney, *J. Geophys. Res.*, 2007, **112**, D09302.
5. C. P. Rinsland, A. Goldman, E. Mahieu, R. Zander, J. Notholt, N. B. Jones, D. W. T. Griffith, T. M. Stephen and L. S. Chiou, *J. Geophys. Res.*, 2002, **107**, ACH 24-21-ACH 24-29.
6. M. Aydin, M. B. Williams, C. Tatum and E. S. Saltzman, *Atmos. Chem. Phys.*, 2008, **8**, 7533-7542.
7. P. J. Crutzen, *Geophys. Res. Lett.*, 1976, **3**, 73-76.
8. M. Chin and D. D. Davis, *J. Geophys. Res.*, 1995, **100**, 8993-9005.
9. M. K. W. Ko and G. Poulet, Very short-lived halogen and sulfur substances. *In Scientific Assessment of Ozone Depletion*: 2002, Global Ozone Research and Monitoring Project Report No. 47; World Meteorological Organization: Geneva, Switzerland, 2003; Chapter 2.

10. P. L. Hanst, L. L. Spiller, D. M. Watts, J. W. Spence and M. F. Miller, *J. Air Pollut. Control Assoc*, 1975, **25**, 1220-1226.
11. P. D. N. Svoronos and T. J. Bruno, *Ind. Eng. Chem. Res.*, 2002, **41**, 5321-5336.
12. A. K. Z. Steiger, Y.; Pluth, M. D., *Antioxid. Redox Signaling*, 2018, **28**, 1516-1532.
13. S. F. Watts, *Atmos. Environ.*, 2000, **34**, 761-779.
14. C.-L. Lee and P. Brimblecombe, *Earth-Sci. Rev.*, 2016, **160**, 1-18.
15. G. Protoschill-Krebs, C. Wilhelm and J. Kesselmeier, *Atmos. Environ.*, 1996, **30**, 3151-3156.
16. A. J. Kettle, U. Kuhn, M. von Hobe, J. Kesselmeier and M. O. Andreae, *J. Geophys. Res.*, 2002, **107**, ACH 25-21-ACH 25-16.
17. S. A. Montzka, M. Aydin, M. Battle, J. H. Butler, E. S. Saltzman, B. D. Hall, A. D. Clarke, D. Mondeel and J. W. Elkins, *J. Geophys. Res.*, 2004, **109**, D22302.
18. R. Atkinson, R. A. Perry and J. N. Pitts, *Chem. Phys. Lett.*, 1978, **54**, 14-18.
19. M. J. Kurylo, *Chem. Phys. Lett.*, 1978, **58**, 238-242.
20. R. A. Cox and D. Sheppard, *Nature*, 1980, **284**, 330-331.
21. A. R. Ravishankara, N. M. Kreutter, R. C. Shah and P. H. Wine, *Geophys. Res. Lett.*, 1980, **7**, 861-864.
22. C. Wilson and D. M. Hirst, *J. Chem. Soc., Faraday Trans.*, 1995, **91**, 793-798.
23. M. L. McKee and P. H. Wine, *J. Am. Chem. Soc.*, 2001, **123**, 2344-2353.
24. S. O. Danielache, M. S. Johnson, S. Nanbu, M. M. L. Grage, C. McLinden and N. Yoshida, *Chem. Phys. Lett.*, 2008, **450**, 214-220.
25. J. A. Schmidt, M. S. Johnson, Y. Jung, S. O. Danielache, S. Hattori and N. Yoshida, *Chem. Phys. Lett.*, 2012, **531**, 64-69.
26. V. Saheb, M. Alizadeh, F. Rezaei and S. Shahidi, *Comput. Theor. Chem.*, 2012, **994**, 25-33.
27. M.-T. Leu and R. H. Smith, *J. Phys. Chem.*, 1981, **85**, 2570-2575.
28. A. Wahner and A. R. Ravishankara, *J. Geophys. Res.*, 1987, **92**, 2189-2194.
29. C. Lee, W. Yang and R. G. Parr, *Phys. Rev. B*, 1988, **37**, 785-789.
30. J. A. Schmidt, M. Kyte, F. F. Østerstrøm, L. M. T. Joelsson, H. C. Knap, S. Jørgensen, O. J. Nielsen, T. Murakami and M. S. Johnson, *Chem. Phys. Lett.*, 2017, **675**, 111-117.
31. S. M. Murphy, A. Sorooshian, J. H. Kroll, N. L. Ng, P. Chhabra, C. Tong, J. D. Surratt, E. Knipping, R. C. Flagan and J. H. Seinfeld, *Atmos. Chem. Phys.*, 2007, **7**, 289-349.
32. X. Ge, A. S. Wexler and S. L. Clegg, *Atmos. Environ.*, 2011, **45**, 524-546.
33. V. Loukonen, T. Kurtén, I. K. Ortega, H. Vehkamäki, A. A. H. Pádua, K. Sellegri and M. Kulmala, *Atmos. Chem. Phys.*, 2010, **10**, 4961-4974.
34. J. Almeida, S. Schobesberger, and A. Kürten, *et al., Nature*, 2013, **502**, 359-363.
35. K. Kobayashi, T. Kasamatsu, T. Kaneko, J. Koike, T. Oshima, T. Saito, T. Yamamoto and H. Yanagawa, *Adv. Space Res.*, 1995, **16**, 21-26.
36. V. Vinogradoff, F. Duvernay, G. Danger, P. Theulé, F. Borget and T. Chiavassa, *Astron. Astrophys*, 2013, **549**, A40.
37. D. E. Woon, *Icarus*, 1999, **142**, 550-556.
38. Y. You, V. P. Kanawade, and J. A. de Gouw, *et al., Atmos. Chem. Phys.*, 2014, **14**, 12181-12194.
39. A.-J. Kieloaho, H. Hellén, H. Hakola, H. E. Manninen, T. Nieminen, M. Kulmala and M. Pihlatie, *Atmos. Environ.* 2013, **80**, 369-377.

40. M. L. Dawson, V. Perraud, A. Gomez, K. D. Arquero, M. J. Ezell and B. J. Finlayson-Pitts, *Atmos. Meas. Tech.*, 2014, **7**, 2733-2744.
41. D. R. Benson, A. Markovich, M. Al-Refai and S. H. Lee, *Atmos. Meas. Tech.*, 2010, **3**, 1075-1087.
42. J. B. Nowak, L. G. Huey, A. G. Russell, D. Tian, J. A. Neuman, D. Orsini, S. J. Sjostedt, A. P. Sullivan, D. J. Tanner, R. J. Weber, A. Nenes, E. Edgerton and F. C. Fehsenfeld, *J. Geophys. Res.*, 2006, **111**, D17308.
43. A. Parandaman, C. B. Tangtartharakul, M. Kumar, J. S. Francisco and A. Sinha, *J. Phys. Chem. A* 2017, **121**, 8465-8473.
44. S. Sarkar, Monu and B. Bandyopadhyay, *Atmos. Environ.*, 2019, **213**, 223-230.
45. H. Li, J. Zhong, H. Vehkamäki, T. Kurtén, W. Wang, M. Ge, S. Zhang, Z. Li, X. Zhang, J. S. Francisco and X. C. Zeng, *J. Am. Chem. Soc.*, 2018, **140**, 11020-11028.
46. S. Sarkar, S. Mallick, P. Kumar and B. Bandyopadhyay, *Phys. Chem. Chem. Phys.*, 2018, **20**, 13437-13447.
47. J. E. Perez, M. Kumar, J. S. Francisco and A. Sinha, *J. Phys. Chem. A*, 2017, **121**, 1022-1031.
48. M. K. Louie, J. S. Francisco, M. Verdicchio, S. J. Klippenstein and A. Sinha, *J. Phys. Chem. A,* 2016, **120**, 1358-1368.
49. M. Nedić, T. N. Wassermann, Z. Xue, P. Zielke and M. A. Suhm, *Phys. Chem. Chem. Phys.*, 2008, **10**, 5953-5956.
50. K. Suma, Y. Sumiyoshi and Y. Endo, *Science*, 2006, **311**, 1278-1281.
51. S. Aloisio and J. S. Francisco, *Acc. Chem. Res.*, 2000, **33**, 825-830.
52. D. Priem, T.-K. Ha and A. Bauder, *J. Chem. Phys.*, 2000, **113**, 169-175.
53. J. C. Hansen and J. S. Francisco, *Chem. Phys. Chem*, 2002, **3**, 833-840.
54. C. Iuga, J. R. Alvarez-Idaboy and A. Vivier-Bunge, *J. Phys. Chem. A*, 2011, **115**, 5138-5146.
55. P. Arathala, M. Katz and R. A. Musah, *Phys. Chem. Chem. Phys.*, 2020, **22**, 10027-10042.
56. A. Parandaman, J. E. Perez and A. Sinha, *J. Phys. Chem. A* 2018, **122**, 9553-9562.
57. S. Sarkar, B. K. Oram and B. Bandyopadhyay, *Phys. Chem. Chem. Phys.*, 2019, **21**, 16170-16179.
58. D. G. Truhlar and B. C. Garrett, *Acc. Chem. Res.* , 1980, **13**, 440-448.
59. B. C. Garrett and D. G. Truhlar, *J. Chem. Phys.*, 1979, **70**, 1593-1598.
60. Y. P. Liu, G. C. Lynch, T. N. Truong, D. H. Lu, D. G. Truhlar and B. C. Garrett, *J. Am. Chem. Soc.*, 1993, **115**, 2408-2415.
61. M. J. Frisch, G. W. Trucks and H. B. Schlegel, et al., *Gaussian*, Gaussian Inc., Wallingford, CT, 2016.
62. R. Peverati and D. G. Truhlar, *Philos. Trans. R. Soc., A*, 2014, **372**, 20120476.
63. R. A. Kendall, T. H. D. Jr. and R. J. Harrison, *J. Chem. Phys.*, 1992, **96**, 6796-6806.
64. D. E. Woon and T. H. D. Jr., *J. Chem. Phys.*, 1993, **98**, 1358-1371.
65. Y. Zhao and D. G. Truhlar, *Theor. Chem. Acc.*, 2008, **120**, 215-241.
66. P. Arathala and R. A. Musah, *J. Phys. Chem. A* 2019, **123**, 8448-8459.
67. A. Parandaman, M. Kumar, J. S. Francisco and A. Sinha, *J. Phys. Chem. A* 2018, **122**, 6266-6276.
68. P. Arathala and R. A. Musah, *J. Phys. Chem. A*, 2020, **124**, 8292-8304.
69. K. Fukui, *Acc. Chem. Res.*, 1981, **14**, 363-368.
70. M. Kumar and J. S. Francisco, *Chem.-Eur. J.*, 2017, **23**, 2522-2526.

71. T. Zhang, X. Lan, Z. Qiao, R. Wang, X. Yu, Q. Xu, Z. Wang, L. Jin and Z. Wang, *Phys. Chem. Chem. Phys.*, 2018, **20**, 8152-8165.
72. M. Kumar, J. M. Anglada and J. S. Francisco, *J. Phys. Chem. A*, 2017, **121**, 4318-4325.
73. S. Grimme, J. Antony, S. Ehrlich and H. Krieg, *J. Chem. Phys.,* 2010, **132**, 154104.
74. J. Zheng, S. Zhang, B. J. Lynch, J. C. Corchado, Y. Y. Chuang, P. L. Fast, W.-P. Hu, Y.-P. Liu, G. C. Lynch and K. A. Nguyen, *et al. POLYRATE, version2016*, University of Minnesota, Minneapolis, MN, 2016.
75. J. R. Alvarez-Idaboy, N. Mora-Diez and A. Vivier-Bunge, *J. Am. Chem. Soc.*, 2000, **122**, 3715-3720.
76. J. R. Alvarez-Idaboy, N. Mora-Diez, R. J. Boyd and A. Vivier-Bunge, *J. Am. Chem. Soc.*, 2001, **123**, 2018-2024.
77. C. Iuga, J. R. Alvarez-Idaboy and A. Vivier-Bunge, *Chem. Phys. Lett.*, 2010, **501**, 11-15.